Available online at www.sciencedirect.com
ScienceDirect
European Journal of Mechanics B/Fluids 26 (2007) 193–219

Evolution of wide-spectrum unidirectional wave groups in a tank: an experimental and numerical study

L. Shemer *, K. Goulitski, E. Kit

Department of Fluid Mechanics, Faculty of Engineering, Tel-Aviv University, Tel-Aviv 69978, Israel

Received 13 February 2006; received in revised form 9 May 2006; accepted 30 June 2006

Available online 1 September 2006

Abstract

Evolution of unidirectional nonlinear wave groups with wide spectra is studied experimentally and numerically. As an example of such an evolution, focusing of an initially wide wave train that is modulated both in amplitude and in frequency, to a single steep wave at a prescribed location along the laboratory wave tank is investigated. When numerous frequency harmonics arrive at the focusing location in phase, a very wave steep single emerges. The experimental study was carried out in two wave flumes that differ in size by an order of magnitude: a 330 m long Large Wave Channel in Hanover, and in 18 m long Tel-Aviv University wave tank. The spatial version of the Zakharov equation was applied in the numerical simulations. Detailed quantitative comparison is carried out between the experimental results and the numerical simulations. Spectra of the 2nd order bound waves are calculated using the theoretical model adopted. It is demonstrated that with the contribution of bound waves accounted for, a very good agreement between experiments and simulations is achieved.

Keywords: Nonlinear water waves; Freak waves; Zakharov equation; Spatial evolution; Bound (locked) waves

1. Introduction

Generation of very steep waves in wave tanks enables experimental study of the wave damage potential and is thus of great importance. Excitation of a single steep wave at a prescribed location in a laboratory wave tank of constant depth is also often required for model testing in coastal and ocean engineering. It is well known that such waves can be generated by focusing a large number of waves at a given location and instant. Dispersive properties of deep or intermediate-depth surface gravity waves can be utilized for this purpose. Since longer gravity waves propagate faster, a wave group generated at the wave maker in which wave length increases from front to tail may be designed to focus the wave energy at a desired location. Such a wave sequence can be seen as a group that is modulated both in amplitude and in frequency. One-dimensional theory describing spatial and temporal focusing of various harmonics of dispersive gravity waves based on the linear Schrödinger equation was presented by Pelinovsky and Kharif [1]. They suggested such a focusing as a possible mechanism for generation of extremely steep singular waves. However, the experiments of Brown and Jensen [2] demonstrated that nonlinear effects are essential in the evolution of those

* Corresponding author. Tel.: +972 3 6408128; fax: +972 3 6407334.
E-mail address: shemer@eng.tau.ac.il (L. Shemer).

0997-7546/$ – see front matter
doi:10.1016/j.euromechflu.2006.06.004

waves. An extensive review of field observations of very steep, the so called freak, or rogue, waves, as well as of the relevant theoretical, numerical and experimental studies was recently presented by Kharif and Pelinovsky [3].

The essentially nonlinear behavior of wave groups with high maximum wave steepness has been demonstrated in a number of studies. Attempts were made to describe the propagation of deep or intermediate depth gravity water-wave groups with a relatively narrow initial spectrum by a cubic Schrödinger equation (CSE). Shemer et al. [4] demonstrated that while CSE is adequate for qualitative description of the global properties of the group envelope evolution, such as focusing that is observed for water waves in sufficiently deep water, it is incapable of capturing more subtle features, for example the emerging front-tail asymmetry observed in experiments. For the weakly-dispersive wave groups in shallow water, application of the Korteweg–deVries equation provided results that were in very good agreement with the experiments [5]. In the case of stronger dispersion in deeper water, models that are more advanced than the CSE are required, since due to nonlinear interactions, considerable widening of the initially narrow spectrum can occur. The modified Schrödinger equation derived by Dysthe [6] is a higher (4th) order extension of the CSE, where the higher order terms account for finite spectrum width [7]. Application of this model indeed provided good agreement with experiments on narrow-band wave groups on relatively high wave steepness [8]. A numerical and experimental study of evolution of bichromatic wave field based of the Dysthe equation was performed by Trulsen and Stansberg [9]. An alternative theoretical model that is free of band-width constraints is the Zakharov equation [10] that takes into account all quartet (Class I) interactions among spectral harmonics in the wave field [11]. Unidirectional spatial version of this equation was derived in Shemer et al. [11] and applied successfully to describe the evolution of nonlinear wave groups in the tank. Kit and Shemer [12] showed the relation between the spatial versions of the Dysthe and the Zakharov equations. In particular, it was demonstrated in this study that the dispersion term in the unidirectional spatial deep-water Dysthe equation is exact, contrary to the temporal version of this equation [13]. The additional linear dispersion terms in [13] stem from the fact that for deep-water waves, the wave frequency ω is related to the wave number k by $\omega = \sqrt{gk}$, thus the Taylor expansion of the frequency difference has an infinite number of terms. In the spatial formulation, the relevant parameter is the wave number difference that is exact and does not contain frequency terms beyond quadratic.

An attempt to check the limits of applicability of the Dysthe equation to describe spatial evolution of wave groups with wider spectrum has been carried out by Shemer et al. [8]. Numerical solutions of the wave group spatial evolution problem were carried out using both Dysthe and Zakharov equations. The obtained results demonstrated that while the Dysthe model performed in a satisfactory fashion for not too wide spectra, it failed for wave groups with initially wide spectra.

Excitation of a single steep wave by focusing is based on superposition of a number of harmonics, each having a moderate steepness that can easily be generated by a wavemaker, that arrive at a prescribed location with identical phases, so that the amplitude of the resulting wave is a sum of amplitudes of all frequency components. Focusing is therefore more effective when the number of free wave harmonics initially generated at the wavemaker is large. Excitation of single wave with extreme amplitude thus requires wide spectrum of the initial wave group generated at the wavemaker. Extremely steep (freak) wave therefore can be seen as wave group with very narrow envelope and correspondingly wide spectrum.

Some preliminary results of all experiments carried out in the Tel-Aviv University (TAU) wave tank and in the Hanover Large Wave Channel (GWK) were presented in [14,15]. Reasonable agreement between measurements and model computations based on the spatial version of the Zakharov equation [8] suggested that the general approach is valid. Focusing was indeed observed close to the designed location, and the variations of the group shape and of the amplitude spectrum along the tank in computations and in experiments were quite similar. The quantitative agreement, however, was insufficiently precise and indicated that further work is necessary. The theoretical model was therefore refined to capture correctly the subtleties of the complicated process of nonlinear interaction among numerous Fourier frequency wave components.

Additional conclusion from our preliminary experiments was that more accurate measurements are required, and that the experimental procedure needs to be revised. Detailed experimental investigation of propagation of steep wave groups with wide spectrum was therefore carried out using a timely opportunity to perform measurements in the 330 m long GWK in Hanover, Germany, which is the largest facility of its kind in Europe. Upon the completion of processing the data accumulated in Hanover it was decided to return to the smaller TAU tank and to perform accurate experiments in this facility.

The study thus was carried out in two wave tanks that differ in size by an order of magnitude, i.e. in the 18 m long TAU wave tank, and in the 330 m long GWK. The experiments are accompanied by numerical simulations based on the modified spatial version of the Zakharov equation.

2. Theoretical background

The purpose of the present study is to obtain at a prescribed distance from the wavemaker, $x = x_f$, a steep unidirectional wave group with a narrow, Gaussian-shaped envelope with the surface elevation variation in time, $\zeta(t)$, given by

$$\zeta(t) = \zeta_0 \exp(-t/mT_0)^2 \cos(\omega_0 t), \tag{1}$$

where $\omega_0 = 2\pi/T_0$ is the carrier wave frequency, ζ_0 is the maximum wave amplitude in the group, and the parameter m defines the width of the group. The small parameter representing the magnitude of nonlinearity ε is the maximum wave steepness $\varepsilon = \zeta_0 k_0$. The wave number k is related to the frequency ω by the finite depth dispersion relation

$$\omega^2 = kg\tanh(kh), \tag{2}$$

g being the acceleration due to gravity. The parameter m determines the width of the group; higher values of m correspond to wider groups and narrower spectra. The spectrum of the surface elevation given by (1) is also Gaussian.

The wave field at earlier locations, $x < x_f$ is obtained from the computed complex surface elevation frequency spectra at these locations. To this end, the unidirectional discretized spatial Zakharov equation based on the version derived in [11] can be used:

$$\mathrm{i}\frac{\mathrm{d}B_j(x)}{\mathrm{d}x} = \sum_{\omega_j+\omega_l=\omega_m+\omega_n} \alpha_{j,l,m,n} B_l^* B_m B_n \,\mathrm{e}^{-\mathrm{i}(k_j+k_l-k_m-k_n)x}, \tag{3}$$

where * denotes complex conjugate and the spatial interaction coefficient $\alpha_{j,l,m,n}$ in its general form is given by

$$\alpha_{j,l,m,n} = V\big(\kappa, k(\omega_l), k(\omega_m), k(\omega_n)\big)\frac{k(\omega_j)-\kappa}{\chi-\omega(\kappa)}, \tag{4}$$

where

$$\kappa = k(\omega_m) + k(\omega_n) - k(\omega_l), \qquad \chi = \omega_m + \omega_n - \omega_l.$$

It can be shown that for deep-water regime for a relatively narrow spectrum, i.e. the quartet nonlinear interactions considered occur among not too distant frequency components, the interaction coefficient approaches the expression used in [11,8]:

$$\alpha_{j,l,m,n} = V\big(k(\omega_j), k(\omega_l), k(\omega_m), k(\omega_n)\big)/c_{g,j}. \tag{4a}$$

In (4), the values of V represent the quartet interaction coefficient in the temporal Zakharov equation as given by Krasitskii [16], and $c_{g,j}$ is the group velocity of the j-th spectral component. Eqs. (3) and (4) accurately describe the slow evolution along the tank of each free spectral component $B_j = B(\omega_j)$ of the surface elevation spectrum in inviscid fluid of constant (infinite or finite) depth.

The dependent variables $B(\omega_j, x)$ in (3) are related to the generalized complex "amplitudes" $a(\omega_j, x)$ composed of the Fourier transforms of the surface elevation $\hat{\zeta}(\omega_j, x)$ and of the velocity potential at the free surface $\hat{\phi}^s(\omega_j, x)$:

$$a(\omega, x) = \left(\frac{g}{2\omega}\right)^{1/2} \hat{\zeta}(\omega, x) + \mathrm{i}\left(\frac{\omega}{2g}\right)^{1/2} \hat{\phi}^s(\omega, x). \tag{5}$$

The "amplitudes" $a(\omega_j)$ can be seen as consisting of a sum of free and the bound waves:

$$a(\omega_j, x) = \big[\varepsilon B(\omega_j, x) + \varepsilon^2 B'(\omega_j, x) + \varepsilon^3 B''(\omega_j, x)\big]\exp(\mathrm{i}kx). \tag{6}$$

The higher order bound components B' and B'' can be computed at each location once the free wave solution $B_j(x)$ is known. Only bound waves of the 2nd order resulting from interactions of all possible wave pairs i and j, $i, j = 1, \ldots, N$, are considered here. Those waves have frequencies $\omega_i + \omega_j$ and $\omega_i - \omega_j$. The phase velocity of

these components depends on the parent free waves and cannot be determined using (2). The corresponding formulae, as well as the kernels necessary for their computations are given in [16,17]. Expressions given in the Appendix of [18] are used for computation of the 2nd order bound waves. It can be easily shown that at this order, computations following [16] yield identical results. Inversion of (5) allows computing the Fourier components of the surface elevation $\hat{\zeta}(\omega, x)$. Inverse Fourier transform then yields the temporal variation for the surface elevation $\zeta(x, t)$.

In this paper, the spatial Zakharov equation (3) is used with the modified interaction coefficient (4). The spectrum corresponding to (1) is integrated from the planned focusing location x_f backwards up to the wavemaker at $x = 0$. The waveforms derived from the computed spectra serve as a basis for computations of the wavemaker driving signals that take into the account the theoretical wavemaker transfer function for a given wavemaker shape (piston in Hanover and flap in TAU) with corrections that account for the actual wavemaker response.

3. Experiments in the Large Wave Channel (GWK) in Hanover

3.1. Experimental facility

The Hanover tank has a length of 330 m, width of 5 m and depth of 7 m. Water depth in the present experiments was set to be 5 m. At the end of the wave tank there is a sand beach starting at the distance of 270 m with slope of 30°. The computer-controlled piston-type wavemaker is equipped with the reflected wave energy absorption system. The focusing location in all GWK experiments was set at $x_f = 120$ m from the wavemaker. This was done to eliminate contamination of the results by waves reflected by the far end of the tank. The instantaneous water height is measured using 25 wave gauges of resistance type, which are placed along the tank wall; higher concentration of the wave gauges is in the region of expected focusing of the wave group. For technical reasons, the nearest wave gauge is placed at a distance of about 50 m from the wavemaker. In addition to those gauges, additional wave height sensors are available in the immediate vicinity of the wavemaker.

The calibration was static and performed by filling the tank first to the depth of 6 m and then reducing the depth in steps of 0.5 m to 3.5 m, thus covering the range of surface elevations relative to the undisturbed value from −1.5 m to 1.0 m. The calibration curve for each wave gauge was obtained by best fit to linear dependence. Due to the size of the facility, the calibration procedure usually takes a whole working day. The wave gauges were therefore calibrated only once for each one of the two experimental sessions that lasted for about 2 weeks. It is estimated that the absolute error in the measured instantaneous surface elevation in most cases did not exceed about 1 cm (few probes were identified as consistently yielding results different from those obtained from nearby wave gauges, the results of those probes were discarded). The relative error thus is about 1% for the steepest waves considered and may be higher than that away from the focusing location. Video camera was placed to record the variation of the water surface elevation in the vicinity of the designed focusing location.

A single wave group was excited in each experimental run. The run started only after a sufficient interval from the previous experiment when the water surface was quiescent and all remaining disturbances decayed totally. The reflected wave energy absorption system effectively eliminated the existence of very long waves in the tank and enabled relatively short (about 15 min) intervals between consecutive experimental runs.

The output voltages of all wave gauges, as well as the wavemaker driving signal and the output of the wavemaker position potentiometer that provides information on the instantaneous wavemaker displacement, were sampled at the frequency of 40 Hz/channel. The total sampling duration $\tau = 350$ s. Of this total record, about 100 s (4096 data points) were selected for each data channel for further processing.

3.2. Experimental procedure

The Gaussian energy spectrum of (1) has a shape with the relative width at the energy level of $1/2$ of the spectrum maximum that depends on the value of the parameter m in (1):

$$\frac{\Delta\omega}{\omega_0} = \frac{1}{m\pi}\sqrt{\frac{1}{2}\ln 2}. \tag{7}$$

The value of the group width parameter in all experiments was selected to be $m = 0.6$, so that (7) yields the relative spectrum width $\Delta\omega/\omega_0 = 0.312$, beyond the domain of applicability of the narrow spectrum assumption of the cubic Schrödinger and Dysthe models [8].

The experiments in GWK were carried out with two carrier wave periods, $T_0 = 2.8$ s (carrier wave length $\lambda_0 = 12.1$ m) and $T_0 = 4.34$ s (carrier wave length $\lambda_0 = 25.0$ m), corresponding to dimensionless depths of $k_0h = 2.59$ and $k_0h = 1.26$, respectively. For the shorter carrier wave length, the deep-water dispersion relation is satisfied approximately, whereas for the longer carrier wave the water at wave number corresponding to λ_0 cannot be considered deep. Even for $\lambda_0 = 12.1$ m, since wide-spectrum wave groups were considered, intermediate-depth waves were present. Therefore, in all expressions for the interaction coefficients finite-depth versions were used. The focusing location, x_f, in the GWK experiments was located at the dimensionless distance x_f/λ_0 of about 10 carrier wave lengths from the wavemaker for $\lambda_0 = 12.1$ m, and at half that distance in terms of the wave lengths for $\lambda_0 = 25.0$ m.

3.2.1. Determination of the wavemaker driving signal

As stated in Section 2, the designed temporal variation of the surface elevation at the wavemaker $\zeta_{des}(t) = \zeta(x = 0, t)$ is computed by backward integration of (3) from the focusing location to $x = 0$. For each carrier wave period T_0 and focusing location x_f, the solution of the system of N ODEs (3), N being the total number of wave harmonics considered, is obtained for distances ranging from the wavemaker location at $x = 0$ up to x_f and beyond. The number of free wave harmonics N considered in those computations was in the range from 56 to 76. The wavemaker driving signal is then calculated from ζ_{des} employing the wavemaker transfer function. This function relates the amplitudes and phases of the harmonic wavemaker displacement at a given frequency to the corresponding parameters of the propagating monochromatic wave. For a given wavemaker shape, i.e. piston or paddle, this function can be found using the linear wavemaker theory (see, e.g. [19]). It is well known, however, that for finite amplitude waves significant nonlinear effects may become important (see, e.g. [20,21]). The complex wavemaker transfer function for a given experimental facility is therefore often found empirically by performing a series of experiments on excitation of monochromatic waves.

Such an experimentally obtained wavemaker transfer function was employed in the GWK experiments to calculate the wavemaker driving signal for both carrier wave frequencies and all values of the maximum wave steepness employed. After a series of experiments has been carried out with driving signals obtained in this fashion, it became obvious that the required initial waveform is in fact not faithfully reproduced. The disagreement apparently stems in part from the nonlinear relation between the complicated shape of the temporal variation of the wavemaker displacement and the resulting amplitude of each frequency harmonic of the surface elevation. Due to nonlinearity, the response of the wave field to forcing at different frequencies in the spectrum that has amplitudes of harmonics varying by an order of magnitude may be quite dissimilar to that predicted by the measured transfer function at a constant wavemaker stroke. Nonlinear interactions among various harmonics also contribute to essential deviation of the actually excited wave field from the designed one.

In view of this, an iterative procedure was developed to determine the wavemaker driving signal. The standard transfer function is usually applied to get the initial approximation of the wavemaker driving signal. The resulting wave field is then compared with the designed shape at a single prescribed location and corrected if necessary, separately for each harmonic. This procedure is, however, complicated by the fact that the comparison cannot be carried out in close vicinity of the wavemaker due to presence of evanescent standing modes. An attempt to subtract the contribution of the computed according to the linear wavemaker theory evanescent modes from the measured at the wavemaker wave field proved to be unsatisfactory, presumably due to the nonlinear effects. Since the evanescent waves vanish at distances of the order of the water depth in the tank, it was decided to perform comparison of the designed and the actual wave field away from the wavemaker. As mentioned above, no wave gauges were available in the Hanover experiments at distances shorter than about 50 m. The probe located at the distance of 52.2 m was thus selected for the wavemaker driving signal adjustment.

An example of the actual wavemaker driving signal adjustment procedure is illustrated in Fig. 1 for the carrier wave period $T_0 = 2.8$ s and maximum designed wave steepness at the focusing location $\varepsilon = \zeta_0 k_0 = 0.3$. The ratio of the complex amplitudes of the surface elevation as measured by the selected wave gauge at $x = 52.2$ m, to those computed at this location by the backward integration of (3) starting from the focusing location, is calculated. The ratio of wave amplitudes for each one of 76 frequency harmonics is presented in Fig. 1(a), while Fig. 1(b) shows the corresponding phase differences. The measured amplitudes exceed the required ones by more than 10%; the measured phases deviate notably from the computed ones mainly for higher frequencies in the spectrum. The data of Figs. 1(a), (b) was approximated by a 3rd order polynomial best fit curves that served to correct the input signal. It should be stressed that experience showed that the actual correction should be weaker than that suggested by the

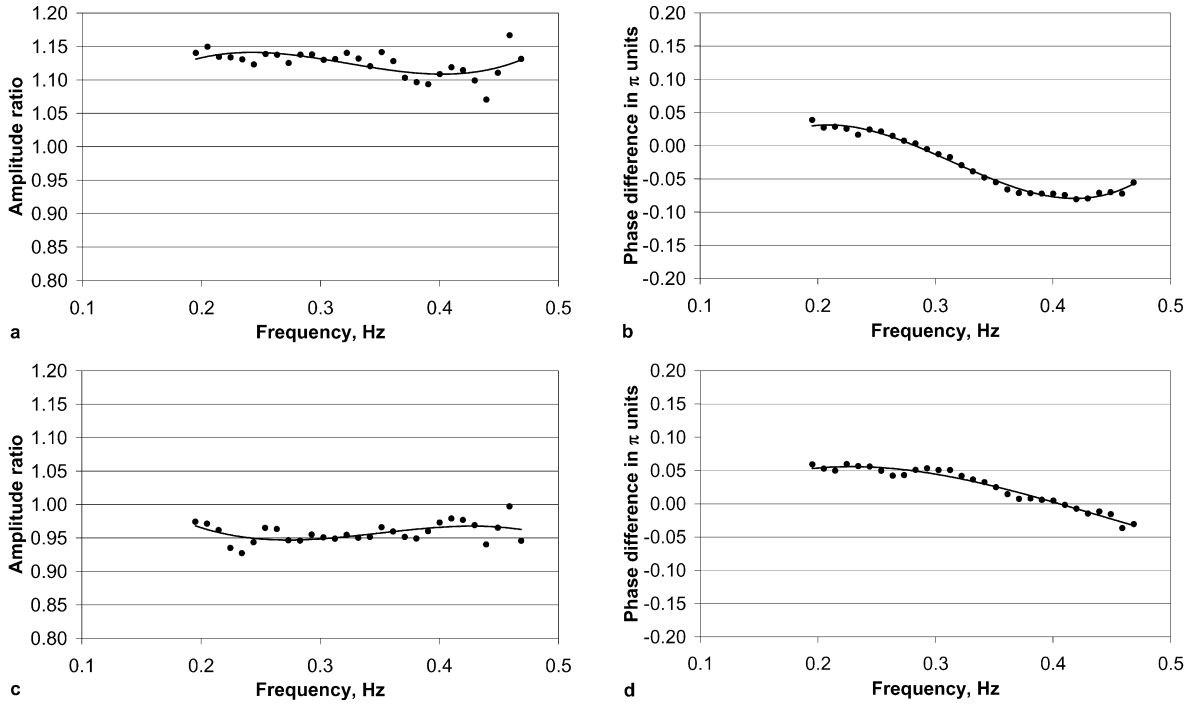

Fig. 1. Wavemaker driving signal adjustment procedure in the GWK experiments for $T_0 = 2.8$ s and $\varepsilon = 0.3$. Relation between the measured at $x = 52.2$ m surface elevation and the corresponding design parameters: (a) amplitude ratio and (b) phase difference in the first approximation; (c) amplitude ratio and (d) phase difference obtained for the actual wavemaker driving signal.

curves on those figures due to a notable overshooting. In any case, for most experimental conditions more than a single iteration was required to get acceptable agreement between the measured and the designed wave forms. Experiments for the conditions of Fig. 1 were finally carried out with the driving signal obtained after 3 iterations that resulted in somewhat better agreement with the designed wave field as shown in Figs. 1(c), (d) (the amplitude difference in the central range of frequencies does not exceed 3–5%). While the resulting signal is still far from being perfect, time limitations intrinsic to use of large experimental facilities prevented us from further attempts to improve the agreement.

Similar procedure was applied for other experimental conditions. It is important to notice that since the adjustments of the wave form had to be made at the distance of about 50 m from the wavemaker, the evolution length up to the focusing location at 120 m from the wavemaker in the GWK experiments was therefore relatively short, being about 6 carrier wave length for $T_0 = 2.8$ s and only about 3 carrier wave length for $T_0 = 4.34$ s.

3.3. Results

Evolution of the wave group shape along the tank is illustrated in Fig. 2(a). The solid line shows the expected variation of the surface elevation, obtained by backward integration of (3) starting from the prescribed Gaussian shape (1) at the focusing location, with the carrier wave period $T_0 = 2.8$ s (frequency $f_0 = 0.357$ Hz) and steepness $\zeta_0 k_o = 0.3$. Computations are carried out for $N = 76$ harmonics, corresponding to frequencies in the range 0.039 Hz $\leqslant f \leqslant 0.76$ Hz. The system of 76 ODEs is solved using the Runge–Kutta procedure with integration step of 5 cm. Test of the integration procedure with the halved integration step of 2.5 cm demonstrated that the solution remains insensitive to step size variation. Surface elevation variation is shown at this figure also for the wavemaker location (actually, the wave gauge is attached at the distance of 5 cm from the piston surface), and for $x = 52.2$ m, location of the wave gauge that served for the wavemaker driving signal adjustment. The results of measurements by the corresponding wave gauges are also plotted by a thin broken line. Note that as the time reference in this and all figures that follow, the instant of the beginning of the wavemaker motion is used.

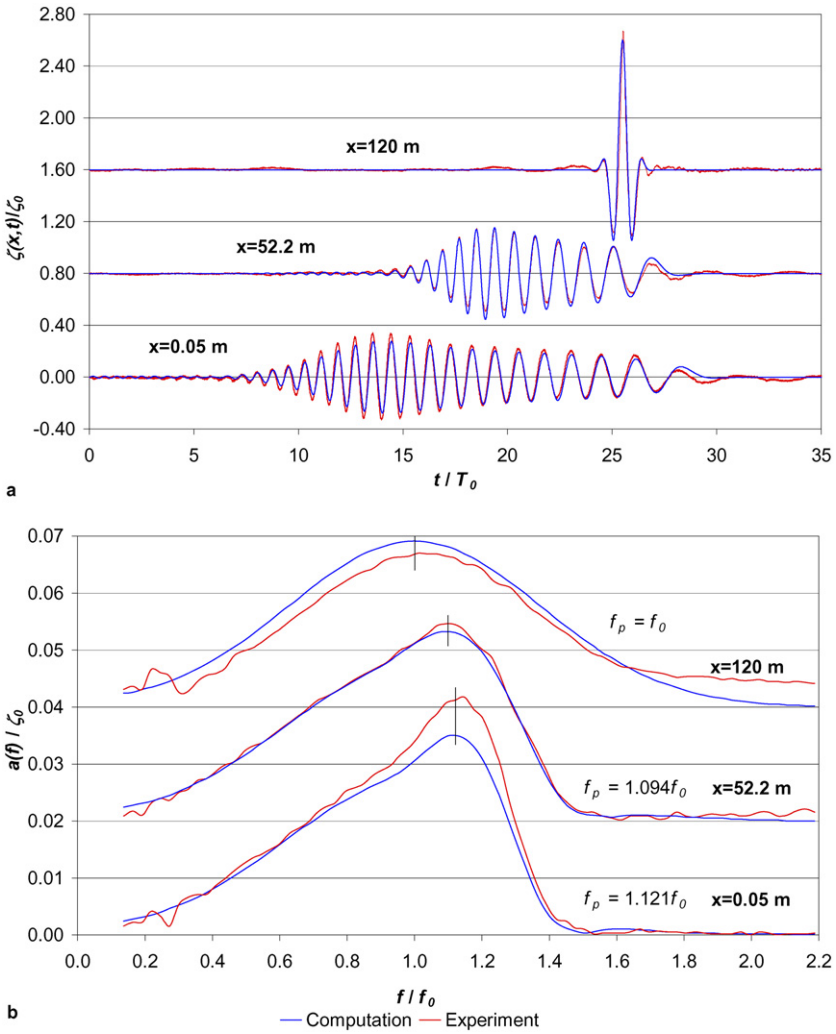

Fig. 2. Evolution of the wave group along the GWK for $T_0 = 2.8$ s and $\varepsilon = 0.3$. (a) Temporal variation of the surface elevation at various locations along the tank; (b) the corresponding amplitude spectra and the peak frequencies.

The agreement between the water elevation measurements and the corresponding computations in Fig. 2(a) is quite good even though only free wave components are accounted for in the computations. The selected value of $m = 0.6$ in (1) yields indeed a narrow wave group with a single steep wave at the focusing location that is obtained when an initially wide wave group gets narrow as it propagates along the tank. The length of waves within the group at the generation location is gradually increasing, and the envelope shape there appears to be quite complicated, in contrast to the symmetric Gaussian shape at the focusing. The group envelope shape is also reproduced well in the numerical simulations. This agreement is particularly good for $x = 52.2$ m, since the adjustment of the wavemaker driving signal has been carried out by comparison of experiments and computations at this location. The maximum wave crest height above the mean water level that is about 0.2 m at the wavemaker increases to more than 0.6 m at the focusing location. The agreement of experiments and computations is less impressive at the wavemaker, most probably due to effect of the evanescent modes. At the focusing location the results of the measurement exhibit a crest that is notably higher than the computed value. Disagreement also manifests itself in some asymmetry of troughs at $x = 120$ m, as well as in long waves that are clearly seen in the wave gauge output.

It should be stressed that focusing can basically be obtained due to simple interference of linear propagating dispersive waves [1]. To asses the effects of nonlinearity, comparison of the computed and the measured amplitude

spectra of the surface elevation at the same locations is carried out in Fig. 2(b). The computed and the measured spectra are discrete and the continuous lines in this and in the following figures are used for convenience due to the large number of frequency harmonics f_i considered. The frequency resolution is determined by the decrement $\Delta f = 1/\tau$, where τ is the measurement duration in the experiments or in the computations. The dimensional discrete amplitudes $a_i = a(f_i)$ are normalized by the maximum designed amplitude at the focusing location, ζ_0. The spectra are shown for the range of frequencies that are excited by the wavemaker. Both measured and computed spectra exhibit significant change of shape along the tank. The peak frequency is shifted to a lower value, and the whole spectrum becomes wider as the group moves along the tank. Note that the differences between the spectra at $x = 0.05$ m and $x = 52.2$ m are relatively minor, indicating that as long as the maximum wave height within the group remains small, the nonlinear interactions are weak and the variation of the group shape results mainly from the linear dispersion. Nonlinearity becomes dominant as the maximum wave height increases with approach to the focusing location, and the spectrum at $x = 120$ m is very different from those measured for a wider group closer to the wavemaker.

As in Fig. 2(a), the agreement between the computed and the measured spectra is the best, although not perfect, for the adjustment location of $x = 52.2$ m. The measured amplitudes at the wavemaker are considerably higher than the computed ones, especially in the vicinity of the peak frequency. This disagreement can be attributed to the appearance of evanescent modes, as well as to local nonlinear effects related to finite wavemaker stroke, and therefore is not discussed here. Most interesting, however, is the notable difference between experiments and computations at the focusing location that manifests itself practically at all frequencies. The ratio between the measured spectral amplitudes and the numerically obtained ones is particularly large at higher frequencies, exceeding about 0.6 Hz. To account for this discrepancy, the contribution of the 2nd order bound waves as defined by (6) is computed.

The effect of the bound waves at the focusing location is studied in Fig. 3 for two cases: for the carrier wave period $T_0 = 2.8$ s with the maximum wave steepness $\varepsilon = 0.3$ (Figs. 3(a) and 3(b)); and for $T_0 = 4.34$ s and $\varepsilon = 0.2$ (Figs. 3(c) and 3(d)). Temporal variation of the surface elevation (Figs. 3(a) and 3(c)) and the amplitude spectra (3(b) and 3(d)) are considered in both cases. All figures also include results for the free waves only for the Gaussian distribution (1). For comparison, experimental results at $x = 120$ m are shown. In addition, the contribution of bound waves computed for the Gaussian wave field is plotted, as well as combined computed effect of free and bound waves. Incorporation of the contribution of bound waves leads to a notable improvement in agreement with the experiments, as can be observed in all figures. In particular, the steep wave crests become sharper and their height increases, so that the computed shape approaches closely the one experimentally obtained. Similarly, the troughs of the wave are flattened, again resulting in a better agreement with the experiments.

Importance of inclusion of bound waves in the analysis becomes even more obvious when amplitude spectra are considered. For both sets of wave group parameters in Fig. 3, as a result of the phase relations between the free and the bound waves, incorporation of bound waves causes substantial decrease in the total wave amplitude for the corresponding frequencies and renders the agreement between experiments and computations nearly perfect. The peak amplitude is shifted to a somewhat higher value, again in agreement with experimental observations. For frequencies exceeding the peak value, bound waves contribute to increase in the total amplitude, although the agreement here is less impressive.

Figs. 3(b) and 3(d) also demonstrate that the contribution of bound waves in the wide-spectrum wave field is qualitatively different from the narrow free wave spectrum case. For a narrow spectrum wave field, the existence of bound waves is manifested at frequencies in the vicinity of the 2nd harmonic of the carrier frequency, as well as at very low frequencies (zeroth harmonic). As a result of that, the spectral overlapping of free and bound components is minimal, thus allowing their straightforward separation in the measured spectrum, as demonstrated in Shemer et al. [11,8]. For the free wave spectrum considered here, however, interactions among remote harmonics lead to emergence of bound waves at frequencies $f_i \pm f_j,\ i, j = 1, \ldots N$, thus covering all frequencies in the range $0 \leqslant f \leqslant 2f_{\max}$, $f_{\max} = f_N$ being the maximum frequency in the free wave spectrum considered. Consequently, bound waves affect the spectral shape also close to the peak frequencies, thus making the division of the total measured wave field to free and bound components more complicated.

The contribution of the 2nd order bound waves considered here is supposed to increase with the nonlinearity parameter ε. Examination of Fig. 3 reveals, however, that relative contribution of bound waves in Figs. 3(c), 3(d), where the maximum wave steepness is $\varepsilon = 0.2$, is more pronounced than that in Figs. 3(a), 3(b) with $\varepsilon = 0.3$. It is known that

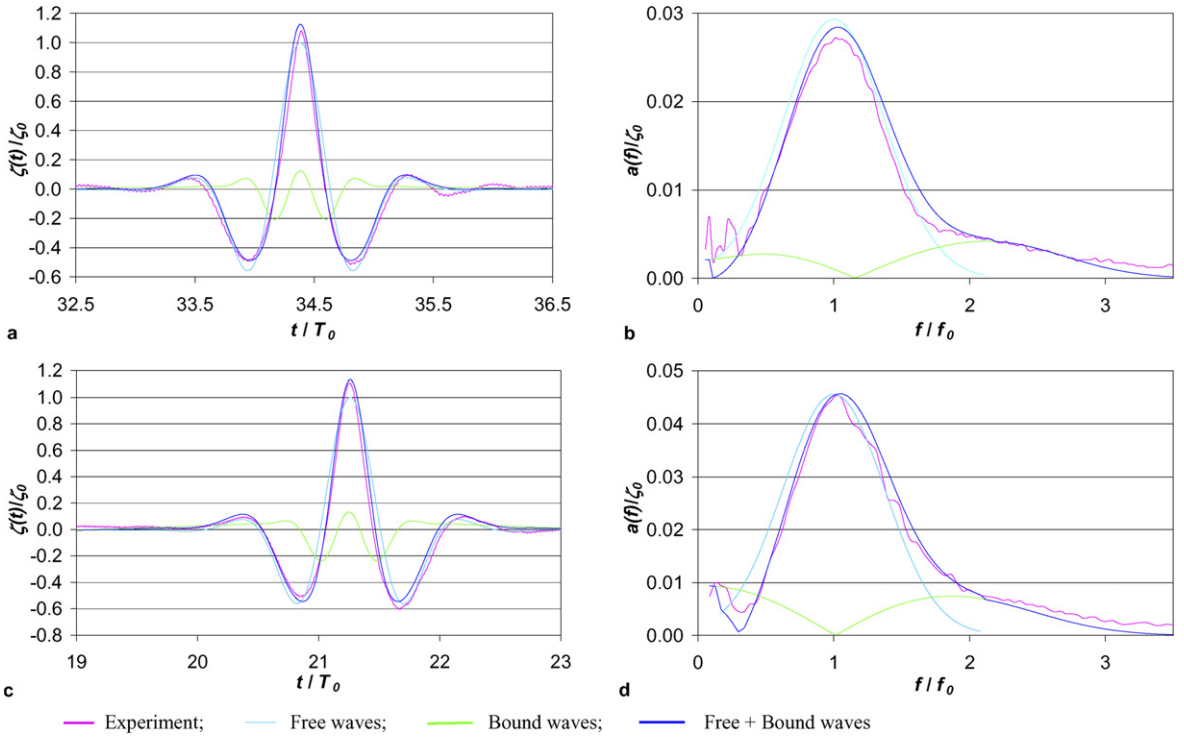

Fig. 3. The effect of the bound waves at the focusing location in the GWK: (a) surface elevation and (b) amplitude spectra for $T_0 = 2.8$ s and $\varepsilon = 0.3$; (c) surface elevation and (d) amplitude spectra for $T_0 = 4.34$ s and $\varepsilon = 0.2$.

for a given wave steepness, contribution of bound waves increases with decreasing depth. The dimensionless water depth based on the carrier wave in Figs. 3(a), 3(b), $k_0h = 2.60$, results in effectively deep water conditions for the dominant part of the spectrum, whereas in Figs. 3(c), 3(d), $k_0h = 1.26$ and the majority of the free harmonics in the spectrum belong the intermediate depth range.

Variation of the computed bound wave contribution to the total wave field with the distance from the wavemaker is studied in Fig. 4 for the surface elevation and in Fig. 5 for the corresponding amplitude spectra. The analysis is carried out for wave groups with the maximum steepness of $\varepsilon = 0.3$ and carrier wave period $T_0 = 4.34$ s. Figs. 4 and 5 demonstrate that the contribution of bound waves cannot be neglected throughout the whole length of the tank. The character of this contribution, however, varies considerably. Bound waves contribute most to the surface elevation variation when the instantaneous free wave height within the group is high. The contribution of bound waves is therefore spread over the whole duration of the unfocused wave group at $x = 0$, and becomes more concentrated as the wave group focuses at $x = 120$ m. For an unfocused group, bound wave contribution to the amplitude spectrum is spread almost uniformly over all frequencies, Figs. 5(a), (b). Double-peaked spectral shape of the bound waves gradually emerges as the wave group focuses (Fig. 5(c)); at the focus location, Fig. 5(d), the contribution of bound waves to the amplitude spectrum is maximal at zero and twice carrier wave frequencies, while at the carrier frequency the spectral amplitude of bound waves vanishes.

In Fig. 6 the difference between the measured amplitudes and the computed ones is plotted for the central part of the spectrum for different locations along the tank for $T_0 = 2.8$ s and $\varepsilon = 0.3$. The contribution of bound waves is taken into account in this figure. Since the differences are small and therefore subject to considerable scatter, 2nd order polynomial trend lines are also plotted. The results of Fig. 6 indicate that difference between computations and measurements gradually grows as the wave group propagates along the tank. Moreover, this difference appears to increase with frequency. These results suggest that dissipation, albeit weak, cannot be totally neglected in the numerical simulations. Since the dissipation in the boundary layers at the tank walls and bottom is relatively weak, it is sufficient to account for the wave energy loss along the tank by adding an additional linear term to the governing

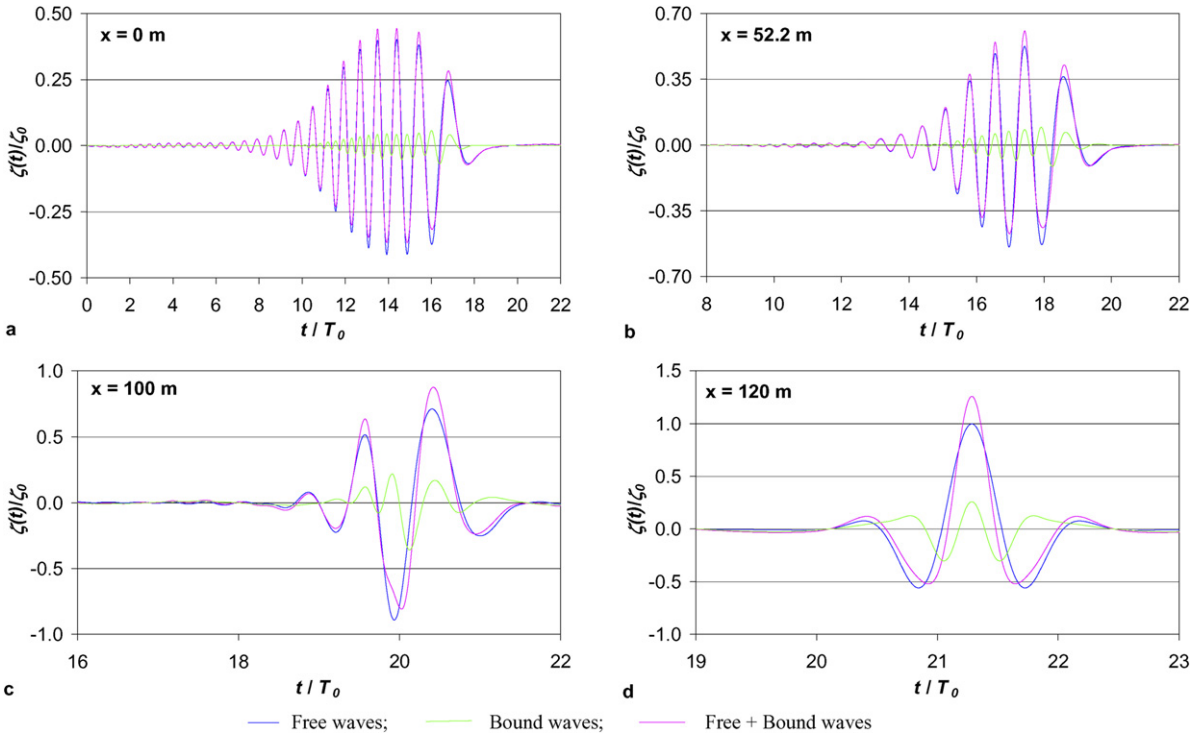

Fig. 4. Variation of the contribution of the bound wave to the surface elevation along the tank computed for the GWK conditions with $T_0 = 4.34$ s and $\varepsilon = 0.3$.

equation, as suggested for gravity-capillary waves by Shemer and Chamesse [22]. The spatial Zakharov equation (3) that accounts for dissipation along the tank can thus be written as

$$\mathrm{i}\frac{\mathrm{d}B_j(x)}{\mathrm{d}x} = \sum_{\omega_j+\omega_l=\omega_m+\omega_n} \alpha_{j,l,m,n} B_l^* B_m B_n \,\mathrm{e}^{-\mathrm{i}(k_j+k_l-k_m-k_n)x} - \gamma_j B_j(x). \tag{3a}$$

The complex dimensional dissipation coefficient γ for a wave of an arbitrary frequency ω in a channel of width w and depth h that results from the Stokes layer at the side walls and the bottom of the tank was given in [23]

$$\gamma = \frac{k}{w\sqrt{\omega/\nu}} \frac{2(\sinh 2kh + kw)}{\sinh 2kh + 2kh} \exp\left(\frac{-\mathrm{i}\pi}{4}\right). \tag{8}$$

Application of (8) yields for the present experimental conditions the following values of the viscous dissipation coefficient: $\gamma = 0.134 \times 10^{-3}\,\mathrm{e}^{-\mathrm{i}\pi/4}$ m^{-1} for the carrier wave period $T_0 = 2.8$ s, and $1.50 \times 10^{-5}\,\mathrm{e}^{-\mathrm{i}\pi/4}$ m^{-1} for $T_0 = 4.34$ s. The expected decay of amplitude at the carrier wave period T_0 for the distance of 120 m is about 1.6% for the shorter wave and about 0.9% for the longer wave. Viscous dissipation becomes thus noticeable only for the high frequency part of the spectrum.

At least two factors thus can be specified that contribute to deviation of the experimentally measured wave field at the focusing location from the Gaussian shape: less than perfect agreement of the excited by the wavemaker wave group with the designed shape, as demonstrated in Fig. 3, and wave energy dissipation along the tank. Both these factors could not be fully accounted for in the course of the experimental sessions in the Hanover tank due to the limited time available. The accuracy of the theoretical model with the modifications included can be examined on the basis of the available experimental data if the experimentally measured temporal variation of the surface elevation at the selected location is chosen as the initial data. For the reasons specified above, it was decided therefore to apply the model computations starting from the complex wave spectrum measured at $x = 52.2$ m. These wave amplitudes, however, have to include the free harmonics only, whereas the measured wave field comprises both free and bound waves. While the bound wave field can be easily computed for any given free wave spectrum, see Figs. 4, 5, the inverse problem is more complicated, and requires an iterative solution.

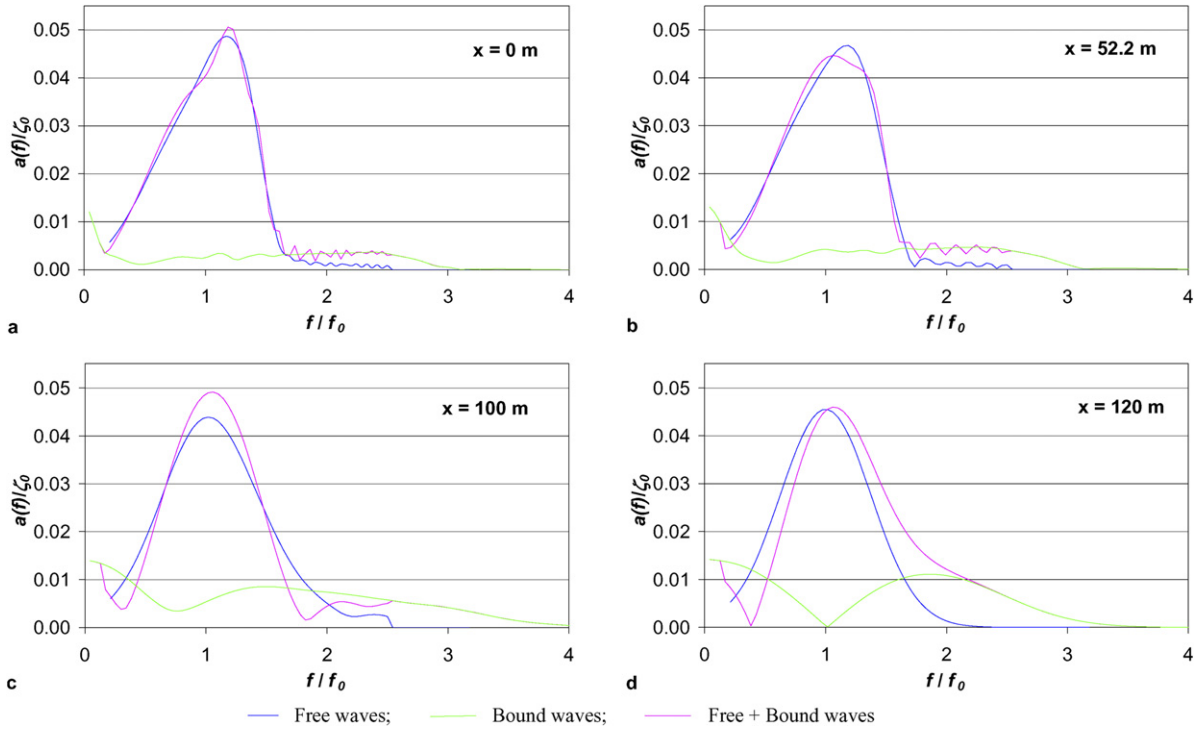

Fig. 5. As in Fig. 4, for the amplitude spectra.

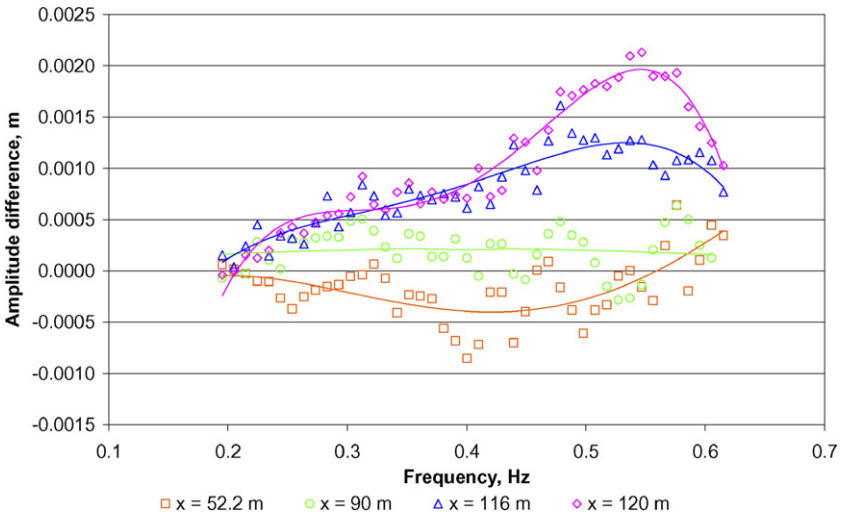

Fig. 6. Difference between the measured and the computed amplitudes for $T_0 = 2.8$ s and $\varepsilon = 0.3$.

Such an iterative procedure is employed here for determining the free wave field from the measured data. The procedure is illustrated in Fig. 7 for the case of the carrier wave period $T_0 = 4.34$ s and $\varepsilon = 0.3$. The first approximation is based on the measured complex wave amplitude spectrum, the absolute values of those amplitudes are presented in Fig. 7(a). It is assumed that the part of this spectrum in the frequency range $0.029\ \text{Hz} \leqslant f \leqslant 0.57\ \text{Hz}$ constitutes the free wave spectrum. The complex 2nd order bound wave spectrum is then computed based on this assumption. These bound waves are then subtracted from the total wave field, new complex free wave spectrum is calculated, and then the total wave field consisting of free and bound waves is obtained. The contributions of the bound waves to the spectrum and to the surface elevation thus calculated are also presented in Figs. 7(a), (b), respectively. The difference

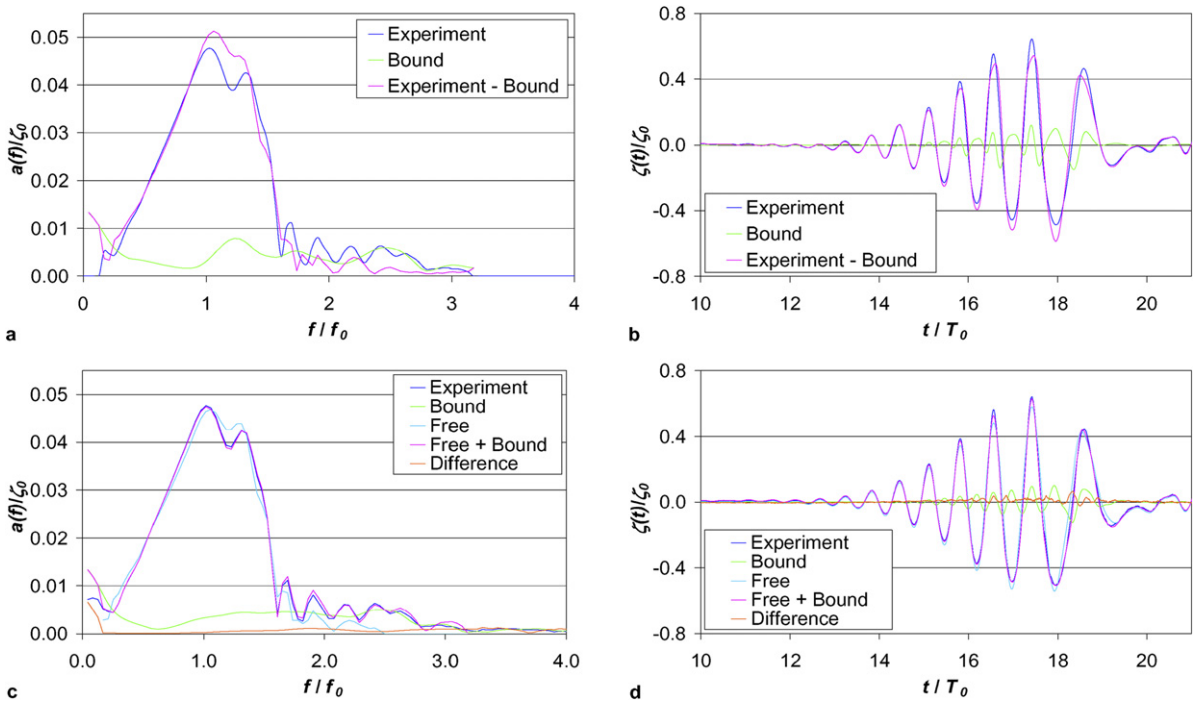

Fig. 7. Determination of the free wave field from the measured in the GWK data for $T_0 = 4.34$ s and $\varepsilon = 0.3$. Initial estimate of the bound and free wave fields at $x = 52.2$ m for (a) amplitude spectra and (b) surface elevation; (c) and (d) show the corresponding results after 4 iterations.

between the measured and the computed complex spectra is then calculated for each frequency in the range considered, and added to the previously assumed free wave spectrum, yielding the next iteration. Iterations are continued until a reasonable agreement between the total measured wave field and the combined wave field resulting from the complex free wave spectrum obtained at the last iteration and the corresponding bound waves is attained. Figs. 7(c), (d) show the results of such a procedure obtained after 4 iterations. In most cases, 3 to 4 iterations are sufficient to get the difference between the measured and the computed surface elevation that is within the experimental error, i.e. less than about 1 cm.

Attempt to excite steep wave with parameters of the previous figure resulted in wave breaking close to the focusing location. Since the analysis of wave breaking is beyond the scope of the present study, it was decided to reduce the wave amplitude by 10% and to perform again the adjustment procedure of the wavemaker driving signal for maximum wave steepness of $\varepsilon = 0.27$. The variation of the surface elevation along the tank is presented in Fig. 8, while the corresponding amplitude spectra are given in Fig. 9. In all figures, results are presented for the driving signal adjustment location, $x = 52.2$ m, for the focusing location at $x = 120$ m, as well as for two location at identical distances of 20 m from the focusing: before the focusing at $x = 100$ m, and after the focusing at $x = 140$ m. In all figures, experimental results are compared with model computations with and without bound waves.

Examination of Fig. 8 reveals that quite a good agreement between model and experimental results is obtained for all locations, and the agreement is notably improved when bound waves are accounted for. At the focusing location, the deviation of the measured wave form from the symmetric computed shape is within the accuracy of the measurements. Note that the wave group shapes at equal distances from the focusing are close to mirror image symmetry. While weak dissipation incorporated in the model computations does not affect the results significantly, it is sufficient to "spoil" the perfect mirror symmetry that is obtained at equidistant from the focus locations in computations without dissipation.

The amplitude spectra enable a more convenient assessment of the accuracy of agreement between experiments and computations. Again, good agreement between measurements and computations is obtained, and incorporation of bound waves' contribution is essential throughout the whole range of frequencies. It is obvious from Fig. 9, however, that the driving signal obtained in the proposed adjustment procedure results in the computed free wave spectral shape at the focusing location that deviates from the original Gaussian.

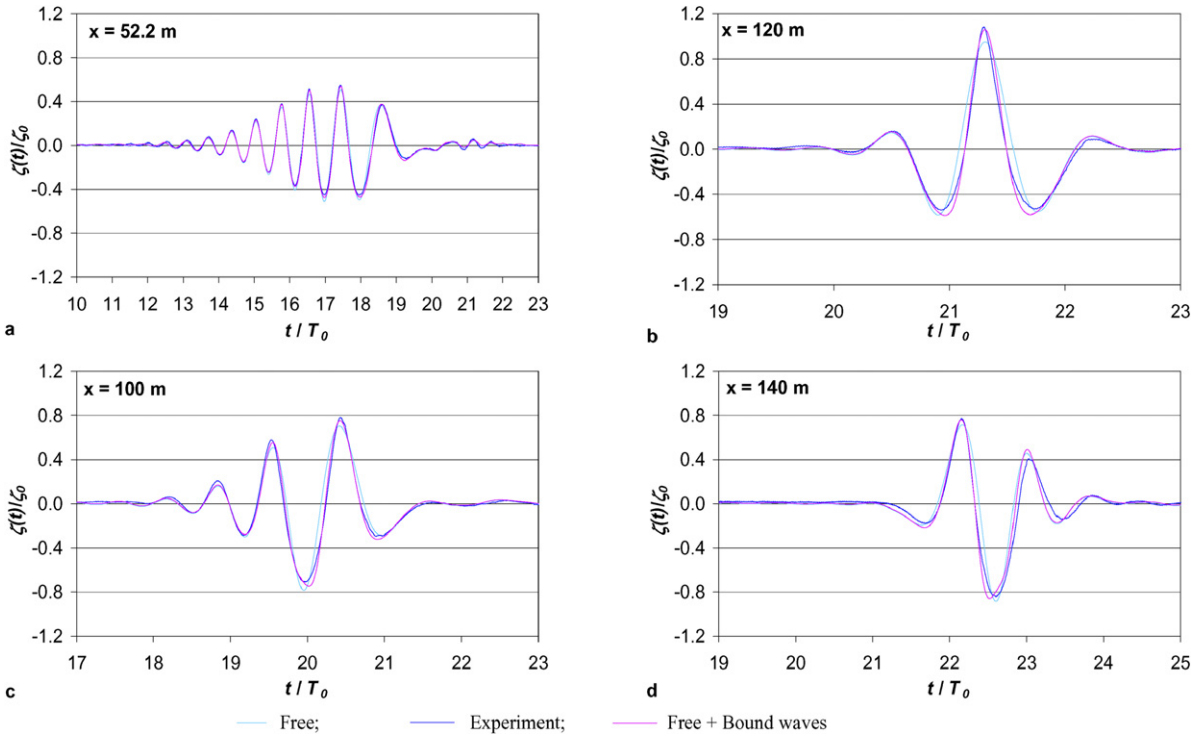

Fig. 8. Comparison of the measured and the computed surface elevations at various locations along the GWK for $T_0 = 4.34$ s and $\varepsilon = 0.27$.

3.4. Summary of the Large Wave Channel (GWK) experiments

The GWK experiments demonstrate that computations of the wave field evolution with wide spectrum based on the adopted version of the spatial Zakharov equation provide a good agreement with the measurement results. More detailed examination reveals some quantitative differences between experiments and computations. These differences can be attributed to some objective problems associated with carrying out experimental studies in such a facility as the Large Wave Channel in Hanover. The experience gained in the GWK study allows specifying the advantages and disadvantages of large scale laboratory experiments. The main advantage is probably the possibility to generate single waves with height exceeding 2 m. The ability to excite waves of this height is certainly important for numerous practical applications where an interaction of waves with structures is considered. The present study, however, is aimed at better understanding of the general features of spatial evolution of essentially nonlinear wave groups with wide spectra. In this respect, a large facility has several important limitations.

(i) For a meaningful study of spatial evolution it is desirable to have an evolution length as large as possible in terms of the dominant wave length. The adopted wave period of 2.8 s was the shortest possible, taking into account the technical limitations of the GWK wavemaker which has a heavy 5 m by 7 m piston and therefore is limited to relatively low frequencies. This limitation becomes even more important since the purpose of the present study was to investigate groups with wide spectra that had to include frequencies much higher than that of the carrier wave. The distance of 120 m from the wavemaker to the focusing location is therefore about 10 carrier wave lengths for $T_0 = 2.8$ s and less than 5 carrier wave lengths for $T_0 = 4.34$ s.

(ii) The flexibility of running experiments in a large facility is necessarily limited. In particular, the locations of the wave gauges have to be determined in advance, and cannot be adjusted in the course of the experiments. The lack of possibility to cover the distances from the wavemaker up to the distance of about 50 m in the prefixed in the present experiments probe layout proved to be of major importance due to the necessity to adjust the wavemaker driving signal at distances where evanescent modes decayed sufficiently, and effectively limited the evolution span from the planned 120 m to about half that length.

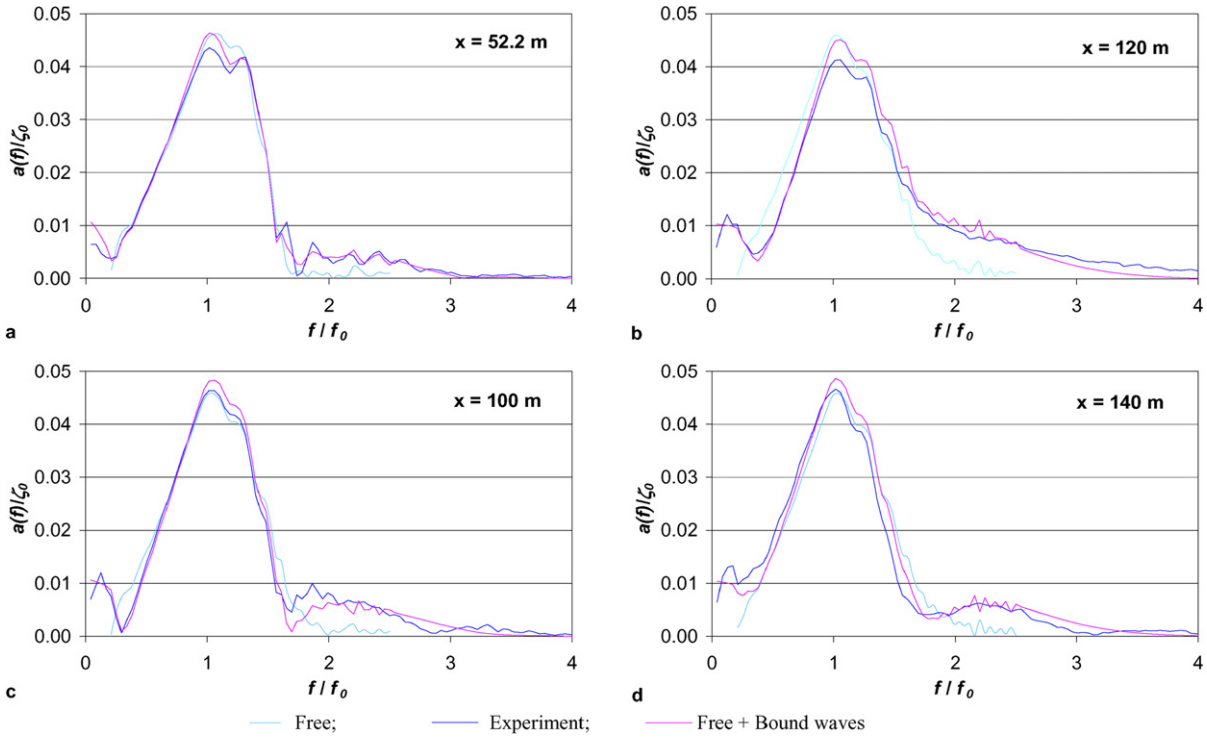

Fig. 9. As in Fig. 8, for the amplitude spectra.

(iii) The calibration procedure takes a whole day, is quite costly due to necessity to pump large volumes of water, and thus can be carried out only once, in the beginning of every experimental session that can be about two weeks long. As a result, the accuracy of the measurements is not always satisfactory, and some probes proved to yield clearly erroneous results.

(iv) Most importantly, access to such a large facility is necessarily limited in time and expensive. On the other hand, the duration of each experimental run is quite considerable, so that only a limited number of runs can practically be performed. Many conclusions regarding the desired modifications in the experimental parameters can only be drawn after processing the accumulated data. Such processing apparently cannot be completed while running the experiments. This poses a limit on a degree of accuracy in comparison with the model computations that can be achieved.

Based on the extensive experience gained in running experiments in the GWK and processing the results, it was decided therefore to carry out measurements in a much smaller wave tank in the Tel-Aviv University, where many drawbacks of the GWK experiments could be eliminated.

4. Experiments in the Tel-Aviv University (TAU) wave tank

4.1. Description of the facility and selection of experimental parameters

The TAU wave tank is 18 m long, 1.2 m wide and has the water depth of 0.6 m. A flap-type wavemaker hinged near the floor is located at one end of the tank, while a wave-energy absorbing sloping beach is located at the far end of the tank. Depth variation due to sloping beach starts at a distance of about 15 m from the wavemaker. The instantaneous surface elevation is measured simultaneously by five resistance-type wave gauges. For better sensitivity the probes used in the present study are made of a pair of blackened platinum wires that have diameter of 0.4 mm. The probes are mounted on a bar parallel to the side walls of the tank at a distance of 0.4 m between the adjacent probes and fixed to a carriage which can be moved along the tank. The probes are statically calibrated in situ using a stepping motor and a computerized calibration procedure described in detail in [24]. The calibration is performed at the beginning

and at the end of each experimental run. The calibration range for each run is adjusted to the expected maximum wave height. The probe response is essentially linear for the range of surface elevations under consideration in the present study. As a result of the calibration procedure, a 2nd order curves relating each probe's output voltage to its immersion depth is obtained. The maximum calibration error is estimated not to exceed 0.2 mm.

The purpose of the experiments was to reproduce in this smaller facility, as close as possible, the dominant dimensionless parameters of the GWK experiments. Additional cases, corresponding to nearly-deep water conditions that are not attainable in the GWK were studied as well. The designed wave group shape at the focusing location is identical to that of the Hanover experiments, and is given by (1) with $m = 0.6$. The maximum wave steepness in the experiments ranges from 0. 1 to 0.4, most runs were performed for $\zeta_0 k_0 = 0.3$. A number of carrier wave periods T_0 was employed. It seems reasonable to perform experiments in both facilities for identical dimensionless water depth defined by $k_0 h$. The values of $k_0 h$ of 2.6 and 1.26 used in Hanover yield for the TAU tank depth of 0.6 m carrier wave lengths of 1.45 m and 2.99 m, respectively. Since the effective length of the tank is about 15 m, and the focusing location has to be sufficiently far from the beach to alleviate contamination of results by the reflected long wave components that cannot be effectively absorbed by the beach, quantitative experiments on the focusing of wave groups with wide spectra and with the carrier wave length of about 3 m that correspond to intermediate depth cannot be carried out. It was thus decided to limit the similarity in the experimental conditions of the experiments in both tanks to the case with $k_0 h = 2.6$, somewhat below the customarily adopted limit of the validity of deep water approximation $kh = \pi$ [19], thus extending the TAU tank experiments to nearly-deep water conditions. The shortest carrier wave period employed in these experiments was $T_0 = 0.6$ s (carrier wave length of 0.56 m, $k_0 h = 6.71$), so that the deep water conditions are satisfied even for most of the low frequency part of the spectrum. The selection of the shortest carrier wave period is based on the following considerations. On one hand, experiments with shorter waves in a tank of a given length allow longer dimensionless (in carrier wave lengths) evolution distances, thus enabling observation of considerable evolution of wave group shape and spectrum. On the other hand, longer evolution distances and higher frequencies result in quite small wave amplitudes at the wavemaker, making it difficult to reproduce faithfully by the wavemaker motion the computed complex waveform that is supposed to serve as the initial condition.

4.2. Wavemaker driving signal

Viscous dissipation along the tank was accounted for in computations of the required surface elevation at the TAU tank wavemaker. The wavemaker driving signal adjustment procedure described in Section 3.2.1 was employed here. Since measurements in this smaller tank can be carried out at any desired location, it was decided to perform the driving signal adjustment by comparing the computed and the measured signal at the distance of 1 m from the wavemaker. This distance that is nearly twice the tank depth is sufficient for the evanescent standing modes to decay; it leaves, however, sufficient evolution range where computations and measurements of the evolving nonlinear wave field can be compared.

The results of this adjustment procedure are illustrated in Fig. 10 for the carrier wave period $T_0 = 0.97$ s, $k_0 h = 2.56$, maximum wave steepness $\zeta_0 k_0 = 0.3$ and the designed focusing location $x_f = 10$ m. The measured at $x = 1$ m temporal variation of the surface elevation is presented in Fig. 10(a). In the same figure, the surface elevation computed by the backward integration of (3a) starting with the initial condition (1) at x_f is also shown. In computations, bound waves of the 2nd order were taken into account. No significant differences between the computed and the measured wave group shape can be discerned in this figure. For comparison, the wavemaker displacement at undisturbed water level which is proportional to the wavemaker driving signal is also plotted on Fig. 10(a). Due to the complicated behavior of the wavemaker transfer function, the shapes of the driving signal and of wave group are notably different. This difference can be even more clearly seen when the corresponding amplitude spectra are compared in Fig. 10(b). Large amplitudes of the wavemaker displacement are required to reproduce faithfully low frequencies of the wave field. Fig. 10(b) also shows the measured and the computed surface elevation spectra at two locations, $x = 0.2$ m and $x = 1.0$ m. The deviations between the calculations and measurements are significantly larger for the location closer to the wavemaker, due to contribution of the evanescent modes.

4.3. Wave group evolution

The wavemaker driving signal adjustment procedure described above resulted in an acceptable agreement of the measured surface elevation in the TAU tank at $x = 1$ m with the computed one for most sets of parameters. This

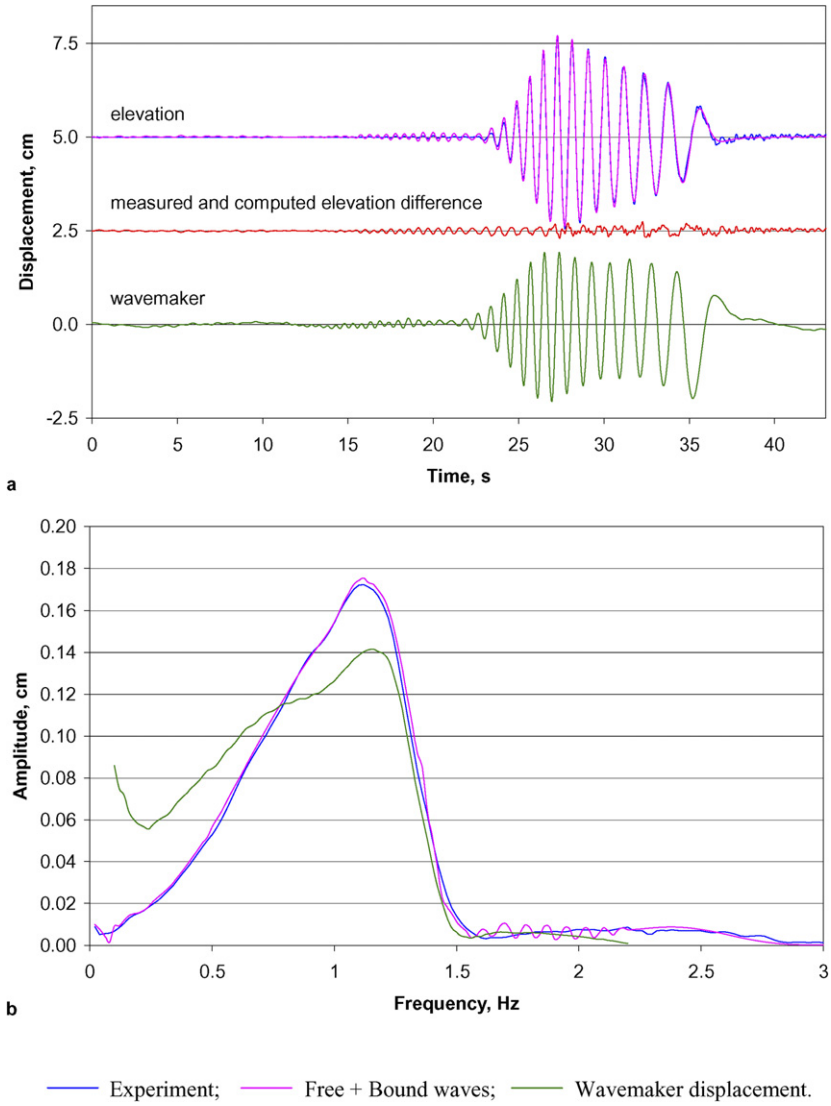

Fig. 10. Results of the wavemaker driving signal adjustment procedure in the TAU tank for $T_0 = 0.97$ s, $\varepsilon = 0.3$: (a) the measured and computed surface elevation, the difference between them, and the wavemaker displacement at $x = 1$ m; (b) the corresponding amplitude spectra.

agreement made it possible to carry out quantitative comparison of wave group evolution along the tank as obtained in experiments, with the model computations based on the backward integration of (3a) starting from the Gaussian envelope shape at the focusing location.

Representative experimental results are given in Figs. 11–13 and compared with those obtained numerically. The computational results presented in those figures include also the contribution of the 2nd order bound waves. In each figure, the variations of the surface elevation and of the amplitude spectra along the wave tank are plotted at 4 locations. The selected locations include the adjustment point at the distance of $x = 1$ m from the wavemaker, the focusing location, as well as two additional positions, one before and one after the focusing. Results are given for three values of the carrier wave period: in Fig. 11 $T_0 = 0.6$ s (carrier wave length 0.562 m, corresponding to dimensionless depth $k_0h = 6.71$), in Fig. 12 $T_0 = 0.85$ s (carrier wave length 1.125 m, with $k_0h = 3.35$), and in Fig. 13 $T_0 = 0.97$ s (carrier wave length 1.45 m, $k_0h = 2.60$, identical to that in the GWK experiments for $T_0 = 2.8$ s). In all those figures the driving amplitudes considered are selected so that at the focusing location, the resulting wave is quite steep, with the maximum wave amplitudes ζ_0 corresponding to the steepness $\varepsilon = k_0\zeta_0 = 0.35$ in Fig. 11 and to $\varepsilon = 0.3$ in Figs. 12 and 13.

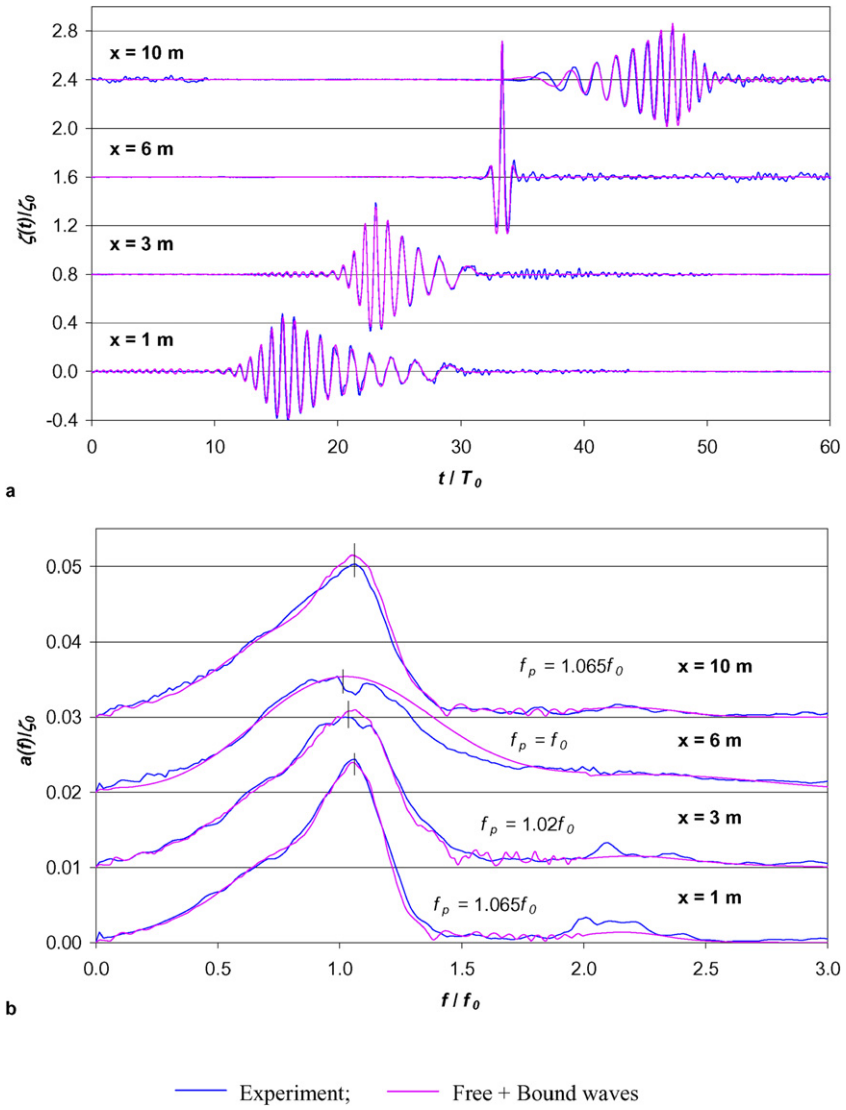

Fig. 11. Comparison of the experimental and computed results at selected locations along the TAU tank for $T_0 = 0.6$ s, $\varepsilon = 0.35$: (a) the surface elevation; (b) the amplitude spectra and the peak frequencies.

In principle, it would be desirable to select the focusing location as far as possible from the wavemaker, to ensure longer evolution domain and lower wave heights at the wavemaker. Preliminary attempts demonstrated that there are difficulties in faithful reproduction of group shapes with very low wave heights. For that reason, for the shortest carrier wave length with $T_0 = 0.6$ s, the focusing distance is 6 m, relatively short compared to the tank length, and constitutes about 10.7 carrier wave lengths. The maximum wave steepness in this case is also chosen to be somewhat higher than that for longer carrier waves. This increase in the initial wave amplitude is aimed to improve the accuracy of results. In computations, 131 frequency harmonics were considered, covering free wave frequency range of $0.125 \text{ Hz} \leqslant f \leqslant 3.375$ Hz. Focusing is designed to occur at larger distances from the wavemaker for longer waves: at $x = 9$ m for $T_0 = 0.85$ s, with 116 free wave harmonics in the range $0.1 \text{ Hz} \leqslant f \leqslant 2.4$ Hz, and at $x = 10$ m for $T_0 = 0.97$ s (106 free harmonics, $0.1 \text{ Hz} \leqslant f \leqslant 2.2$ Hz). Note, however, that in terms of the carrier wave lengths those focusing distances are shorter than in Fig. 11, being 8.0 in Fig. 12 and 6.9 in Fig. 13.

In all cases, a very good agreement between the computed superposition of the free and the 2nd order bound wave fields and the measurement results is obtained for the variation of the wave group shape along the tank. Similarly good agreement is observed in all amplitude spectra in Figs. 11(b)–13(b) for each one of the spectral harmonic. Modulation

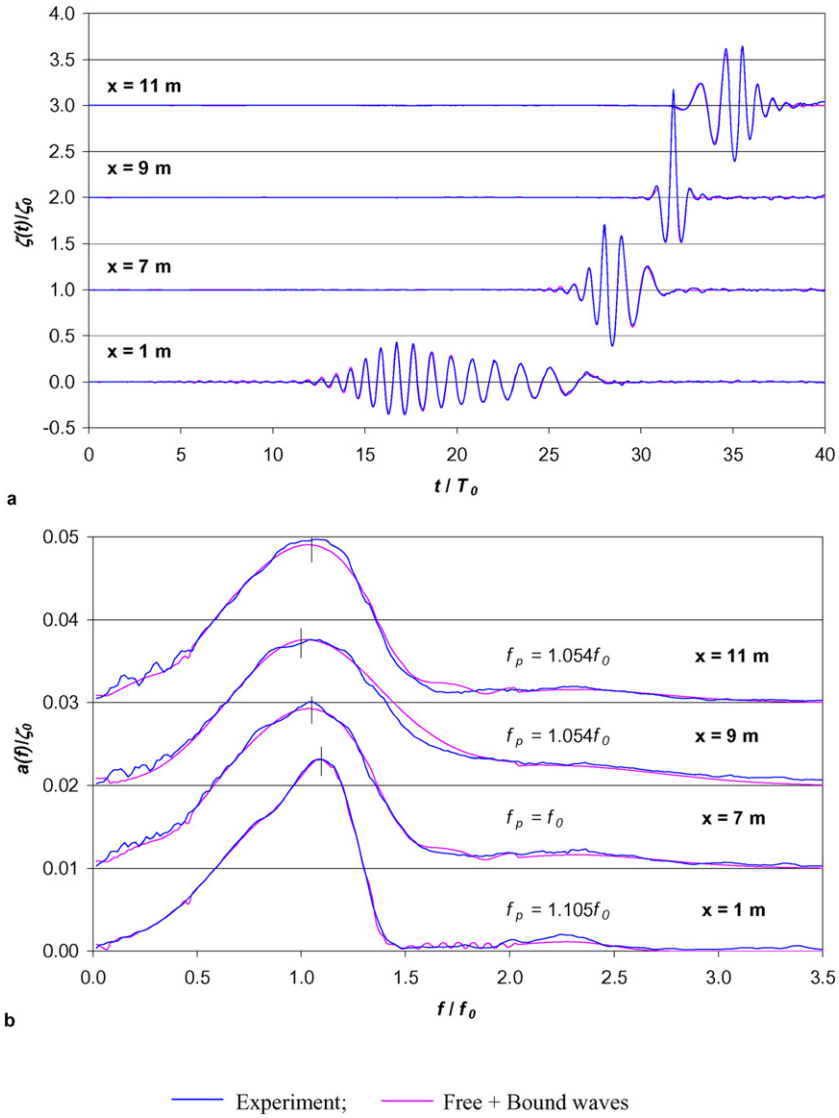

Fig. 12. As in Fig. 11 for $T_0 = 0.85$ s, $\varepsilon = 0.3$.

of the amplitude and the frequency within the group is clearly seen in Figs. 11(a)–13(a) at $x = 1$ m, and the maximum wave amplitude within the group then increases towards the focusing location. At the focusing, a single steep wave with height very close to the designed value is obtained in all cases. Close to the wavemaker, the envelope of the wave group with the shortest carrier wave in Fig. 11(a) is more asymmetric than in the two other cases, where the distance to the focusing location in terms of carrier wave lengths is shorter. In Fig. 12(a), wave group is shown at equal distances of 2 m on both sides from the focusing, at 7 m and 11 m from the wavemaker. One can notice that the two curves exhibit nearly perfect mirror symmetry. The lack of exact symmetry, at least in the computed results, stems from weak dissipation that is introduced into the model computations.

Amplitude spectra at the same locations presented in Figs. 11(b)–13(b) allow estimation of variation of contribution of each harmonic in the course of the evolution. The spectral shape variation in all figures is quite similar, indicating that the variation of dimensionless depth between different cases does not affect the evolution pattern strongly. The spectrum has the maximum width at the focusing location, while close to the wavemaker it is somewhat narrower. The peak frequency drifts in the course of the evolution process. The minimum value of the peak frequency, corresponding to that of the carrier wave, is obtained at the focusing location. The upward shift of the peak frequency from the carrier

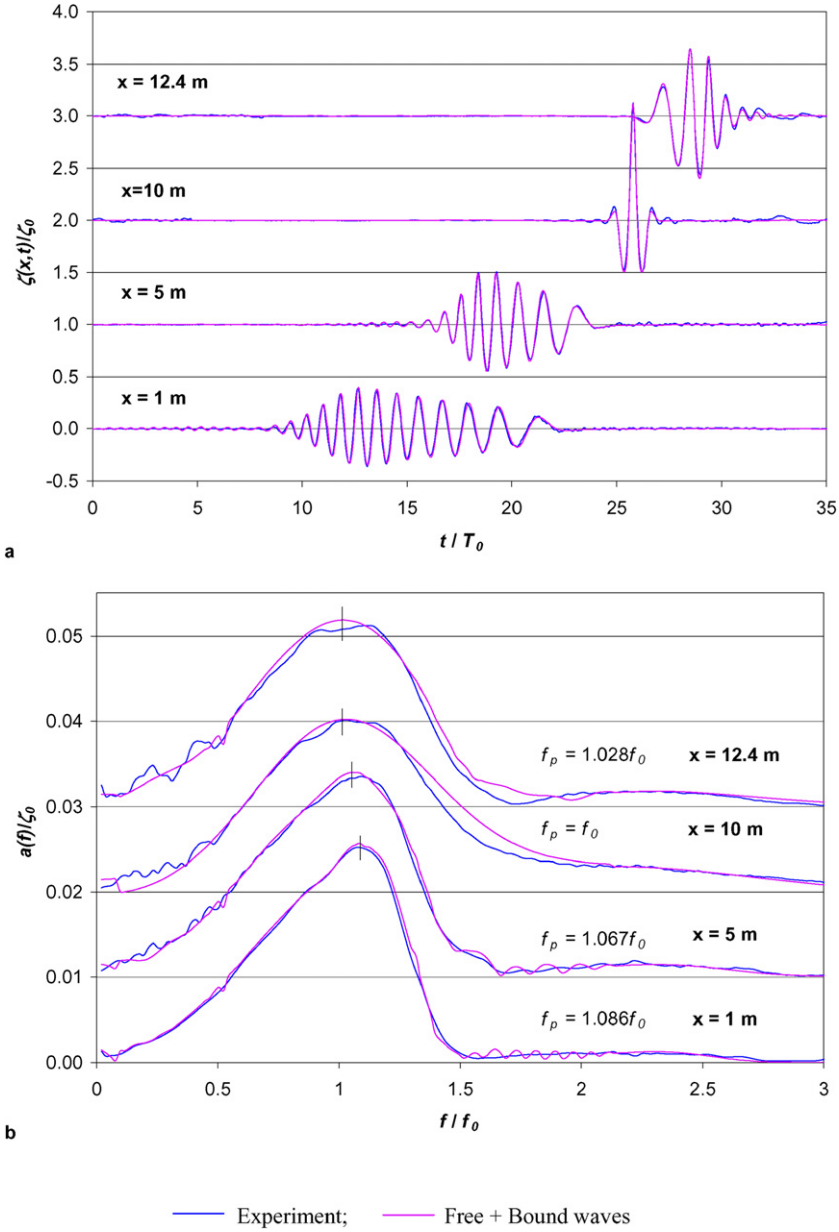

Fig. 13. As in Fig. 11 for $T_0 = 0.97$ s, $\varepsilon = 0.3$.

wave value increases with the distance from the focusing location. The full symmetry of the spectral shapes at equal distances from the focusing is violated by the viscous dissipation; this effect is more visible for free harmonics at higher frequencies.

5. Scaling consideration

Results on evolution of wave groups with wide spectra presented above were obtained in two wave tanks that differ in size considerably. The characteristic wave lengths in those facilities necessarily vary by an order of magnitude, as a result of different wave excitation mechanisms employed that have to be adjusted to the size of the tank. In spite of that, the evolution patterns observed in the experiments and obtained in the numerical simulations are quite similar in both facilities. Those patterns are determined by combination of linear and nonlinear contributions. The effects of

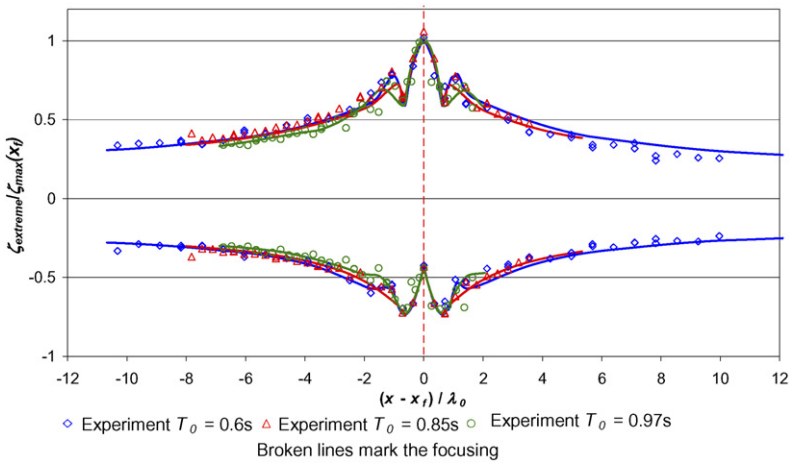

Fig. 14. Extreme values of crest and trough deviations from the undisturbed water level in the TAU tank: experiments vs. computations for $\varepsilon = 0.3$.

nonlinearity depend mainly on the representative wave steepness. In the present study, the maximum wave steepness at the focusing location, $\varepsilon = \zeta_0 k_0$, was selected as the nonlinearity parameter. The values of ε in experiments and computations in both facilities were very close, and the results presented above are mostly for high values of the maximum steepness of about $\varepsilon = 0.3$. Nonlinear effects are most readily identified in the variation of the spectral shapes that would remain constant if nonlinearity was negligible. Results of Sections 3 and 4 demonstrate that the variations of the spectral shape with the distance from the wavemaker obtained in both facilities were essential.

Evolution of the wave group shape along the tank, while being dependent on nonlinearity, is strongly affected by linear effects. The dominant linear effect in the evolution process is dispersion that for gravity waves depends on the dimensionless water depth, kh. Based on the carrier wave length $\lambda_0 = 2\pi/k_0$, the dimensionless water depth was in the range of $2.6 \leqslant k_0 h \leqslant 6.7$ for the TAU tank, and had values of $k_0 h = 2.6$ and $k_0 h = 1.26$ in the GWK experiments. Hence, with the exception of longer carrier wave studies in Hanover, carrier waves can be considered as propagating over deep water in all cases. It should be stressed, however, that since wave groups with wide spectra were considered in this study, the free wave spectrum excited by wavemaker always contained also harmonics that corresponded to quite long and thus weakly dispersive waves. Good agreement demonstrated in the previous sections between experiments and computations in all cases indicates that the spatial evolution model based on the Zakharov equation performs quite well even in these conditions.

Results presented above demonstrate that the amplitude- and frequency-modulated wave groups at the wavemaker, computed by the backward integration of the governing equation, begin with high frequency waves and end with long waves. The wave heights at both ends of the group are quite small. For each experimental facility, there exists a lower limit on the wave heights beyond which waves cannot be with faithfully reproduced. In the present experiments in the TAU tank, the minimum wave height considerations often determined the maximum possible focusing length x_f. These restrictions were considered when it was decided to carry out the experiments for the focusing distances of about $5\lambda_0$ to $10\lambda_0$ in the GWK, and for $6.9\lambda_0$ to about $10.7\lambda_0$ in the TAU tank.

The variety of factors discussed above leads to the dimensionless focusing distances employed in the present study that are not very different in both facilities; the longer is the carrier wave length, the shorter is the dimensionless focusing distance.

The focusing process along the tank can be followed in greater detail if the maximum surface elevation attained at a given location during the passage of the group, or the higher wave crest, is plotted against the distance from the wavemaker. The resulting curve can be seen as the boundary of the wetted surface left by the propagating wave group at the tank side wall. Similarly, the variation along the tank of the deepest wave trough can also be plotted. In order to compare quantitatively the focusing processes for different experimental conditions and in the two facilities, appropriate normalization is required. The propagation distance in each experiment is thus measured relative to the designed focusing location and normalized by the corresponding carrier wave length. The maximum wave crest height above the undisturbed level at the focusing location serves as the normalizing factor for both crest and trough elevations. The computed values that include the contribution of the 2nd order bound waves are used for normalization.

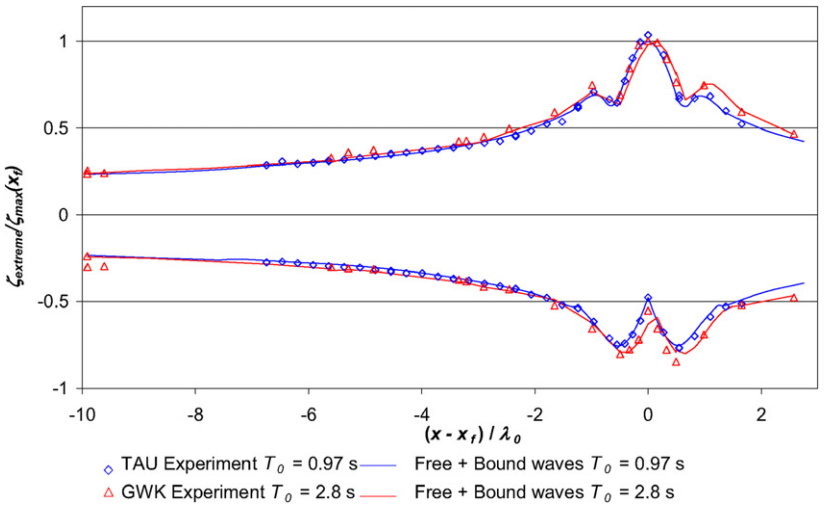

Fig. 15. Comparison of evolution of normalized extreme elevations along both tanks for $k_0h = 2.6$ and $\varepsilon = 0.2$.

The normalized extreme values of wave crest and trough obtained experimentally in the TAU tank at the maximum designed wave steepness of $\varepsilon = 0.3$ for three values of the carrier wave period, $T_0 = 0.6$ s, $T_0 = 0.85$ s and $T_0 = 0.97$ s, are presented in Fig. 14. In the same figure, the corresponding computed quantities are also shown. Good agreement between computations and experiments is obtained for all frequencies. For all cases in Fig. 14, the maximum elevation at the focusing is increased by a factor of about 3 relative to that at the wavemaker, whereas the increase in the through depth is smaller. The rate of decrease of the maximum elevation declines with the distance from the focusing location. Since in all cases the free wave spectra at the focusing location, scaled by the carrier wave period, as well as the nonlinear parameters, are identical, in absence of effects related to water depth, shapes of all curves relative to focusing should also be identical. At distances exceeding about $5\lambda_0$ from the focusing, the rate of decrease of the maximum surface elevation becomes quite slow. All curves in Fig. 14 have a common salient feature: the dependence of the extreme surface elevation on distance from the wavemaker is quite complicated in the vicinity of the focusing location, apparently as a result of interplay of the phases of various harmonics as they approach the same value at the focusing. Note also that at focusing, the maximum trough depth has a local minimum. Hence, the maximum wave height, defined as the difference between the extreme values of the surface elevation at crest and trough, does not attain its maximum value at exactly the focusing location, but rather is shifted and exhibits two maxima at both sides of the focusing. The slight dissimilarity in shapes of curves may be attributed to depth effects.

Closer investigation of the similarity between the shapes is performed in Fig. 15, where comparison is carried out between evolution of normalized extreme elevation along both tanks at identical values of dimensionless depth $k_0h = 2.6$. Computations corresponding to the GWK experiments are performed using the measured complex wave spectrum at the wavemaker adjustment location as the initial condition. To demonstrate that the wave group evolution pattern remains qualitatively similar for a somewhat weaker forcing, the results in this figure are presented for the nonlinearity parameter $\varepsilon = 0.2$. To enable such a comparison, the numerical solution corresponding to TAU conditions was extended beyond the actual wavemaker location to the dimensional distance of $(x - x_f)/\lambda_0 = -9.91$, as in the GWK experiments. The dependencies of both maximum and minimum elevation for both facilities in Fig. 15 collapse on the same curves. The minor differences can be attributed to several factors. First, the effect of dissipation is more pronounced in the TAU tank. Note that dissipation affects not just the amplitudes but also the phases of each harmonic. In addition, the adjustment of the wavemaker driving signal in the GWK experiments was less accurate as specified in above. Fig. 15 also confirms the conclusion from Fig. 14 that the effect of focusing is mainly restricted to the last 5 carrier wave lengths before the focusing point. At larger distances, the extreme values of the surface elevation do not change significantly to justify longer focusing distances from the wavemaker to excite even steeper waves.

The effect of nonlinearity on the focusing process in both facilities is studied in Fig. 16 for two values of the nonlinearity parameter, $\varepsilon = 0.2$ and $\varepsilon = 0.3$. As a reference condition for assessment of the role of finite wave height on the focusing process, the linear solution of the evolution of wave group with the shape given by (1) can be invoked. For the temporal evolution case, the problem of variation of the surface elevation in space of time was obtained by

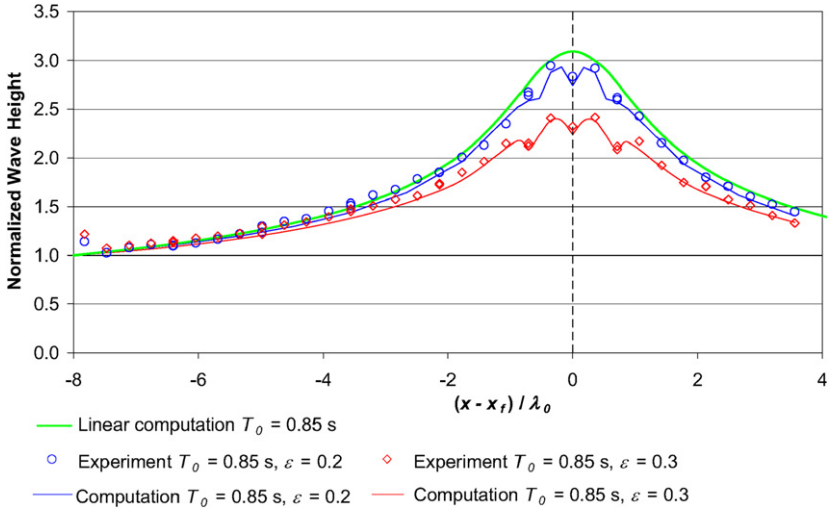

Fig. 16. The effect of nonlinearity on the variation along the tank of the maximum wave height normalized by its value at the wavemaker.

solving the linear Schrödinger equation [2]. It can be easily shown that for the spatial evolution case, this solution can be presented in the following form:

$$\zeta(X,\tau) = \frac{\zeta_0}{\sqrt[4]{1+(X/(2\pi^2m^2))^2}} \exp\left[-\frac{(\tau/(2\pi m))^2}{1+(X/(2\pi^2m^2))^2}\right] \times \cos\left[\frac{(X/2)(\tau^2/(2\pi^2m^2))}{1+(X/(2\pi^2m^2))^2} - \frac{\tan^{-1}(X/(2\pi^2m^2))}{2} + \tau\right] \tag{9}$$

where the dimensionless spatial X and temporal τ variables are related to their dimensional counterparts by

$$X = \omega_0^2 \left.\frac{\mathrm{d}C_g}{\mathrm{d}k}\right|_0 \frac{1}{C_{g,0}^3} x, \qquad \tau = \omega_0\left(t - \frac{x}{C_{g,0}}\right). \tag{10}$$

In (10), the group velocity and its derivative with respect to the wave number k evaluated for carrier wave parameters using the dispersion relation (2) are given by

$$C_{g,0} = \frac{\omega_0}{2k_0}\left(1 + \frac{2k_0h}{\sinh(2k_0h)}\right), \qquad \left.\frac{\mathrm{d}C_g}{\mathrm{d}k}\right|_0 = \omega_0\left[\frac{h}{k_0\sinh(2k_0h)} - \frac{1}{4k_0^2} - \frac{4h^2\sinh^2(k_0h)}{\sinh^2(2k_0h)}\right]. \tag{11}$$

Results on the variation of the maximum wave heights within the group, normalized by the maximum computed wave height at the wavemaker, with the dimensionless distance from the wavemaker, x/λ_0, for various degrees of nonlinearity are shown in Fig. 16 for the carrier wave period $T_0 = 0.85$ s in the TAU tank. This figure clearly demonstrates that the effectiveness of focusing decreases with increase in wave steepness. For the dimensionless focusing distance of about 8 carrier wave lengths, the relative increase in the maximum wave height is close to 3 for $\varepsilon = 0.2$, and remains below 2.5 for $\varepsilon = 0.3$. These values are obtained when contribution of 2nd order bound waves is accounted for. As demonstrated above, bound waves' contribution effectively increases the maximum wave height in the vicinity of the focusing. In spite of the fact that no bound waves are included in the linear solution that is apparently valid for vanishing amplitudes and thus corresponds to the case when $\varepsilon \to 0$, the relative effectiveness of focusing is higher in this case than that obtained for finite amplitudes. Note also that the spatial variation of the maximum wave height obtained from the linear solution is smooth also around the focusing location, in contrast to behavior of the computed and experimental results for finite amplitudes.

Apart of dispersion, dissipation is an additional linear effect that can modify the evolution process. It was assumed in this study that the dominant dissipation mechanism is that due to viscous effects in the oscillating Stokes boundary layer at side wall and, for shallower waves, at the bottom of the wave tank, as well. The corresponding dissipation coefficient γ given by (8) therefore depends on both the depth and the width of the tank, as well as on the wave

frequency. As already mentioned, for the carrier wave periods employed here, in most cases the TAU tank has a larger dimensionless depth than Hanover tank. The 1.2 m width of the TAU tank in terms of carrier wave lengths is much larger than 5 m width of the GWK. Both these parameters contribute to lower effective dissipation in the smaller TAU tank. On the other hand, wave frequencies are much lower in the GWK, leading to wider Stokes layer there and correspondingly lower dissipation coefficients.

For wave groups of a given shape propagating in different facilities, the effect of dispersion on wave group evolution will be the same if the value of k_0h is identical. Similarity in dispersion, however, still does not ensure that effects of dissipation in different facilities also satisfy similarity conditions. To estimate the dissipation effects quantitatively, consider waves with an arbitrary wave number k propagating over constant depth h. The dimensionless energy flux decay in the course of the evolution process up to the distance x from the wavemaker is expressed as $\exp(-2x\gamma)$, where γ is the absolute value of the coefficient calculated using (8). Assuming the same water viscosity ν in both tanks, the ratio of the dimensionless dissipation rates γ/k in the TAU (denoted by the index T) and in the Hanover (denoted by H) wave tanks is obtained from (8) for identical dimensionless water depth $k_\mathrm{T}h_\mathrm{T} = k_\mathrm{H}h_\mathrm{H}$

$$R = \frac{\gamma_\mathrm{T}/k_\mathrm{T}}{\gamma_\mathrm{H}/k_\mathrm{H}} = \frac{\sinh 2k_\mathrm{T}h_\mathrm{T} + k_\mathrm{T}w_\mathrm{T}}{\sinh 2k_\mathrm{H}h_\mathrm{H} + k_\mathrm{H}w_\mathrm{H}} \frac{w_\mathrm{H}}{w_\mathrm{T}} \sqrt{\frac{\omega_\mathrm{H}}{\omega_\mathrm{T}}}. \tag{12}$$

Using the gravity wave dispersion relation for identical dimensionless water depth kh in both tanks, (12) can be rewritten using the dimensionless tank width w/h as

$$R = \frac{\sinh 2k_\mathrm{T}h_\mathrm{T} + k_\mathrm{T}w_\mathrm{T}}{\sinh 2k_\mathrm{H}h_\mathrm{H} + k_\mathrm{H}w_\mathrm{H}} \frac{w_\mathrm{H}/h_\mathrm{H}}{w_\mathrm{T}/h_\mathrm{T}} \frac{h_\mathrm{H}^{3/4}}{h_\mathrm{T}^{3/4}}. \tag{13}$$

For the conditions of the present experiments, it can be easily seen that the first factor in the product in the right-hand side of (13) is always close to unity, so that this ratio can be essentially simplified

$$R = \frac{w_\mathrm{H}/h_\mathrm{H}}{w_\mathrm{T}/h_\mathrm{T}} \left(\frac{h_\mathrm{H}}{h_\mathrm{T}}\right)^{3/4}. \tag{14}$$

The dimensionless decay ratio of two waves with identical dimensionless depth kh in TAU tank and GWK is thus $R = 1/2(5/0.6)^{3/4} = 2.45$. The dimensionless width of TAU facility that is larger than that of GWK by a factor of 2 contributes to a lower decay rate. However, the entire viscous dissipation rate is higher in the TAU tank than in the GWK as a result of notably higher carrier wave frequencies used in a smaller facility to obtain the same dimensionless spectra. Different dissipation rates constitute one of the rationales to conduct experiments in two facilities of essentially different size.

For the Hanover experiments, $x_\mathrm{f}\gamma_0 = 0.016$ for $T_0 = 2.8$ s and $x_\mathrm{f}\gamma_0 = 0.0086$ for $T_0 = 4.34$ s. In the TAU tank, the values of $x_\mathrm{f}\gamma_0$ range from 0.028 for $T_0 = 0.97$ s to 0.035 for $T_0 = 0.6$ s. These values indicate that dissipation is weak but not negligible for all experimental conditions, being, as expected, indeed more pronounced in the smaller TAU tank.

These estimates, carried out for a single frequency, should be validated by experiments on the evolution of the whole wide-spectrum wave group. In the absence of dissipation, the wave energy flux along the tank should be conserved. In the linear approximation, this energy flux can be presented as $\Sigma c_{\mathrm{g},i} a_i^2$, where $c_{\mathrm{g},i}$ and a_i are the group velocity and the amplitude of the ith frequency harmonic, respectively, and the summation is carried out over all free waves in the spectrum.

The variation of energy flux along the tank estimated in the linear approximation from the experiment in both tanks is presented in Figs. 17(a)–(c). In these figures, the corresponding absolute values of the amplitudes are taken either as obtained directly from the corresponding amplitude spectra, or after the contribution of bound waves at the appropriate frequencies is subtracted following the iterative procedure described in Section 3.3, so that the modules of complex amplitudes that contain only free waves are obtained. On the same figures, corresponding computational results, with and without viscous dissipation accounted for, are also presented. To enable quantitative comparison, the computations in all cases are performed starting with the initial conditions corresponding to the measured wave field at the wavemaker driving signal adjustment location.

In all figures, in the absence of dissipation the energy flux is approximately conserved. The "dip" in all curves is observed around the focusing location, indicating that contribution of the nonlinear terms to the energy flux, which is

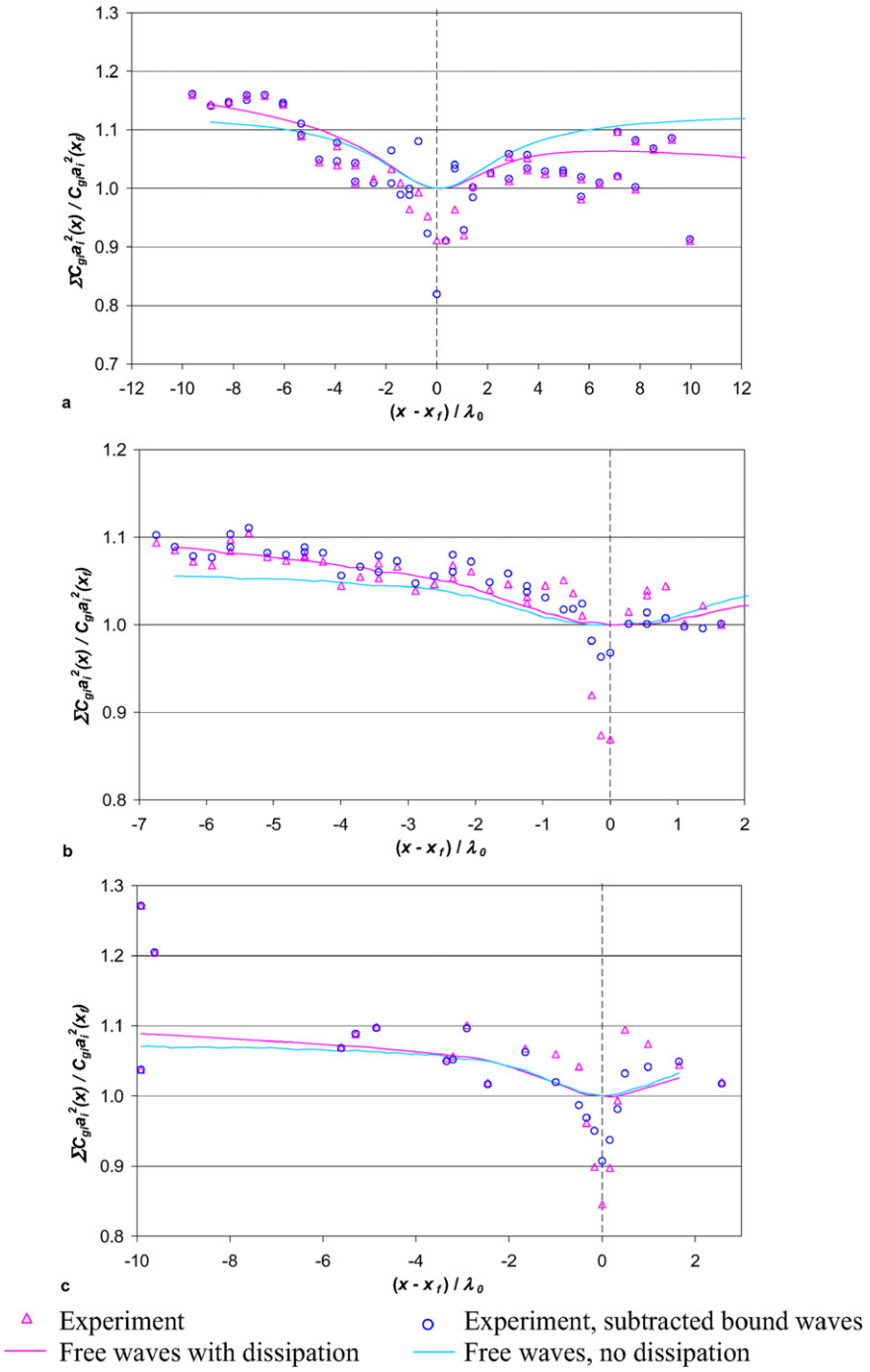

Fig. 17. Variation of the linear part of the energy flux along the tank estimated from the experiments and computed with and without accounting for viscous dissipation. (a) $T_0 = 0.6$ s, $\varepsilon = 0.35$; (b) $T_0 = 0.97$ s, $\varepsilon = 0.3$; (c) $T_0 = 2.8$ s, $\varepsilon = 0.3$.

not accounted for here, becomes more prominent in this region. Contrary to nonviscous case, when viscous dissipation is accounted for, energy flux after the dip does not return to its initial value and continues to decrease along the tank. The experimental results agree well with the viscous computations, showing similar dip around the focusing location. Note that subtraction of the bound waves is essential particularly in the vicinity of focusing, where this operation improves notably the agreement with computational results performed when viscous dissipation is accounted for.

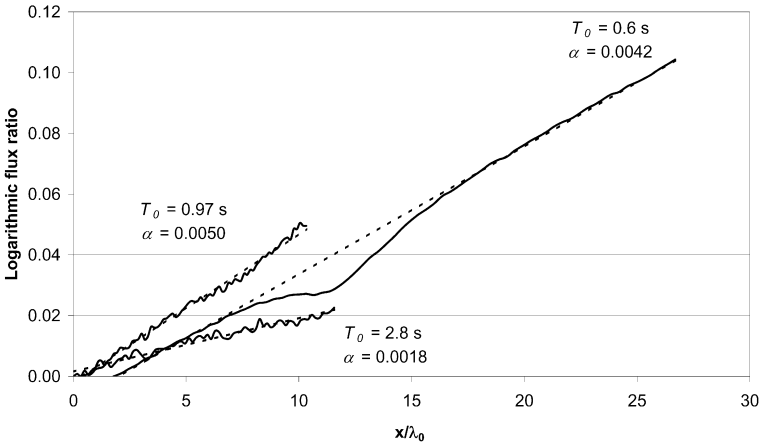

Fig. 18. Rate of energy flux decay along the tank.

Table 1
Linear rates of decay computed for the experimental condition in both tanks

	$T_0 = 0.6$ s $\lambda_0 = 0.562$ m	$T_0 = 0.85$ s $\lambda_0 = 1.125$ m	$T_0 = 0.97$ s $\lambda_0 = 1.453$ m	$T_0 = 2.8$ s $\lambda_0 = 12.1$ m	$T_0 = 4.34$ s $\lambda_0 = 25.0$ m
$\gamma_0\lambda_0$	0.00324	0.00385	0.00411	0.00163	0.00179
a	0.0042	0.0048	0.0050	0.0018	0.0020

The agreement in the energy flux estimates measured in both tanks and those obtained from integration of the viscous nonlinear model, demonstrated in Fig. 17, prompted an attempt to estimate the overall rate of energy flux decay along the tank. To this end, the ratio of the linear part of the total energy flux by all free harmonics, computed without and with viscous dissipation, is calculated. Natural logarithm of this ratio is plotted in Fig. 18 as a function of the normalized by the corresponding carrier wave length longitudinal coordinate. The resulting curves also exhibit a dip around the focusing, but otherwise behave in a close to linear fashion. The slopes of the straight lines, α, plotted by curve fitting, are also shown in this figure. It is instructive to compare these value of α with the dimensionless decay rate $\gamma_0\lambda_0$, where γ_0 is calculated for the corresponding carrier wave length λ_0 using (7). The corresponding rates are given in Table 1.

The results of Table 1 for carrier wave period $T_0 = 0.97$ s in the TAU tank and for $T_0 = 2.8$ s in the GWK that both correspond to $k_0h = 2.6$, are in agreement with estimates based on (11). Table 1 indicates that the decay rate calculated for the carrier wave length give a reasonable estimate of the slopes of the curves in Fig. 18 that take into account all numerous harmonics that participate in the evolution process and exchange energy among them.

6. Conclusions

The validity of the modified version of the unidirectional spatial Zakharov equation for description of evolution along an experimental wave tank of nonlinear wave fields with wide spectrum is verified in this study. Experiments are carried out in two very different experimental facilities for compatible experimental parameters, i.e. the wave group shapes and spectra at the focusing location were kept the same in the TAU tank and in the GWK, and the study was carried out for identical values of the dimensionless maximum wave steepness at the focusing location. Moreover, an effort was made to study wave groups with identical dispersion that is dependent on the dimensionless tanks depths, kh. This effort was only partially successful due to the technical limitations of the experimental facilities, and full dispersion similarity was attained only for a single value of kh (based on the carrier wave parameters). On the other hand, carrying out the study in two very different in size tanks enabled covering a wide range of kh. The dimensionless depths of carrier waves studied ranged from $kh = 1.26$, corresponding to intermediate depth, to $kh = 6.7$, in the deep water range. However, due to the considerable width of the wave group spectra in this investigation, in all occasions,

among the frequency harmonics that constituted the wave field, both strongly- and weakly-dispersive components were present.

The consistent approach was adopted in experiments in both facilities to make it possible to isolate the effect of scaling. It was expected that the scaling effects will be mainly manifested in different dissipation rates in the two tanks. As an example of the evolution problem of a wide-spectrum wave field, focusing of an initially wide wave group due to combined effects of dispersion and nonlinearity is considered. In both facilities, a very large number, often exceeding 100, of free wave harmonics was considered.

Advantages and disadvantages of larger size of the experimental facility are discussed. The dimensionless parameters that determine the effective size of the facility are introduced, and it is shown that under certain conditions, smaller experimental tank that has greater flexibility in running experiments can be advantageous for studies of spatial evolution problems due to higher accuracy of results and possibility to carry out large number of experimental runs at a reasonable price. On the other hand, for many applications the absolute (dimensional) wave height is important. In those cases, bigger facilities offer substantial benefits.

The ability to excite focused steep waves at any desired location along the tank is demonstrated. Large number of wave harmonics is required to generate very steep wave at the focusing location, making the focusing problem suitable for analysis of evolution of wide-spectra wave groups. It is shown that the focusing process is accompanied by a notable change of the spectral shape and is thus essentially nonlinear. The modified unidirectional spatial discrete version of the Zakharov equation as given by (3) and (4a) that takes into account all quartet interactions among the spectral harmonics of the wave field is adequate to describe nonlinear evolution of steep wave groups with wide spectrum propagating in water of constant intermediate depth.

To achieve not only qualitative but also quantitative agreement between the model predictions and the experiments, it is insufficient, however, to consider the nonlinear evolution process of the free wave components only. At least two additional effects have to be accounted for. First, dissipation along the tank may be essential. It is demonstrated that dissipation can be adequately described by an additional linear term in (3) that represents the amplitude decay of each spectral mode as a result of viscous boundary layers at the bottom and side walls of the tank. Analysis of the dissipation effects in both facilities that takes into account the characteristic scales is presented. This analysis demonstrates that the ratio of the dimensionless rates of viscous dissipation for harmonics with identical dispersion as represented by the dimensionless tanks depths, kh, depends on the cross-sectional dimensions of the tank cross-section. For identical values of kh, the wave frequencies in larger facility are substantially lower. Therefore, in spite of the fact that dimensionless width of the TAU tank is larger than that in Hanover, viscous decay is stronger in this smaller tank due to higher frequencies.

Secondly, effects related to the bound waves cannot be neglected. These effects strongly depend on the wave steepness. Second-order bound are accounted for in the present study. While bound waves become particularly important mainly in the vicinity of focusing, they cannot be disregarded closer to the wavemaker as well. While computation of the bound wave field from the known complex amplitude spectrum of free waves is relatively straightforward, the inverse problem of determination of the free wave spectrum from the measured wave field is more complicated. This problem arouses since the accuracy of designed wave field reproduction by the wavemaker in the GWK was not sufficient to carry out quantitative comparison of experimental and computational results. It thus became necessary to estimate the free wave content of the actual wave field excited in experiments in the vicinity of the wavemaker. To this end, an iterative procedure is developed. This free wave field then was used as the initial condition for computations based on the model equations.

When corrections due to 2nd order bound waves and (mainly for the smaller TAU tank) to viscous dissipation are accounted for, very good agreement between experiments and numerical simulations is achieved. This agreement includes variation of the group shape along the tank and changes in amplitudes of each one of the numerous spectral harmonics that constitute the wave field under investigation.

Probably even more sensitive test of the accuracy of the theoretical model applied in the present study is the comparison of the computed and experimentally measured effectiveness of focusing that is defined as the ratio of the maximum surface elevation within the group at the focusing location, to the corresponding value at the wavemaker. It is shown that nonlinear effects tend to decrease this efficiency. It should be stressed that the variation of the maximum surface elevation along the tank critically depends not only on the amplitudes but also on the phases of each spectral harmonic. Very good agreement obtained between experimental results in both facilities and the corresponding com-

putations demonstrates that evolution along the tank of the complex amplitudes at each frequency, and not just of their absolute values, is adequately described by the adopted theoretical model.

It thus can be concluded that the modified version of the unidirectional spatial Zakharov equation can serve as an effective computational model for description of evolution along the experimental wave tanks of wave fields with no limits on their spectral width.

Acknowledgements

This study is supported by a grant # 964/05 from the Israeli Science Foundation. The authors gratefully acknowledge the European Community support under the Access to Research Infrastructures Action of the Human Potential Program (contract HPRI-CT-2001-00157) that made possible experiments in the Large Wave Channel (GWK) of the Coastal Research Center (FZK) in Hanover.

References

[1] E. Pelinovsky, C. Kharif, Simplified model of the freak wave formation from the random wave field, in: T. Miloh, G. Zilman (Eds.), Proc. 15th Int. Workshop on Water Waves and Floating Bodies, Caesaria, 2000, pp. 142-145.
[2] M.G. Brown, A. Jensen, Experiments on focusing unidirectional water waves, J. Geophys. Res. 106 (2001) 16,917–16,928.
[3] C. Kharif, E. Pelinovsky, Physical mechanisms of the rogue wave phenomenon, Eur. J. Mech. B Fluids 22 (2003) 603–634.
[4] L. Shemer, E. Kit, H.-Y. Jiao, O. Eitan, Experiments on nonlinear wave groups in intermediate water depth, J. Waterway, Port, Coastal & Ocean Eng. 124 (1998) 320–327.
[5] E. Kit, L. Shemer, E. Pelinovsky, T. Talipova, O. Eitan, H.-Y. Jiao, Nonlinear wave group evolution in shallow water, J. Waterway, Port, Coastal & Ocean Eng. 126 (2000) 221–228.
[6] K.B. Dysthe, Note on a modification to the nonlinear Schrödinger equation for application to deep water waves, Proc. Roy. Soc. London A 369 (1979) 105–114.
[7] M. Stiassnie, Note on the modified nonlinear Schrödinger equation for deep water waves, Wave Motion 6 (1984) 431–433.
[8] L. Shemer, E. Kit, H.-Y. Jiao, An experimental and numerical study of the spatial evolution of unidirectional nonlinear water-wave groups, Phys. Fluids 14 (2002) 3380–3390.
[9] K. Trulsen, C.T. Stansberg, Spatial evolution of water surface waves: numerical simulation and experiment of bichromatic waves, in: Proc. 11th Int. Offshore and Polar Engrg. Conf., Stavanger, Norway 2001, pp. 71–77.
[10] V.E. Zakharov, Stability of periodic waves of finite amplitude on the surface of deep fluid, J. Appl. Mech. Tech. Phys. 2 (1968) 190–194, (English transl.).
[11] L. Shemer, H.-Y. Jiao, E. Kit, Y. Agnon, Evolution of a nonlinear wave field along a tank: experiments and numerical simulations based on the spatial Zakharov equation, J. Fluid Mech. 427 (2001) 107–129.
[12] E. Kit, L. Shemer, Spatial versions of the Zakharov and Dysthe evolution equations for deep water gravity waves, J. Fluid Mech. 450 (2002) 201–205.
[13] K. Trulsen, I. Kliakhandler, K.B. Dysthe, M.G. Velarde, On weakly nonlinear modulation of waves on deep water, Phys. Fluids 12 (2000) 2432–2437.
[14] K. Goulitski, L. Shemer, E. Kit, Steep unidirectional waves: experiments and modeling, Izv. Vyssh. Uchebn. Zaved. Applied Nonlinear Dynamics 12 (2004) 122–131.
[15] L. Shemer, K. Goulitski, E. Kit, J. Gruene, R. Schmidt-Kopenhagen, On generation of single steep waves in tanks, in: WAVES 2005 – Madrid, Spain, 2005.
[16] V.P. Krasitskii, On the reduced equations in the Hamiltonian theory of weakly nonlinear surface waves, J. Fluid Mech. 272 (1994) 1–20.
[17] M. Stiassnie, L. Shemer, On modification of Zakharov equation for surface gravity waves, J. Fluid Mech. 143 (1984) 47–67.
[18] M. Stiassnie, L. Shemer, Energy computations for coupled evolution of Class I and Class II instabilities of Stokes waves, J. Fluid Mech. 174 (1987) 299–312.
[19] R.G. Dean, R.A. Dalrymple, Water Wave Mechanics for Engineers and Scientists, World Scientific, Singapore, 1991.
[20] O.S. Madsen, Generation of long waves, J. Geophys. Res. 76 (1971) 8672–8683.
[21] R.E. Flick, R.T. Guza, Paddle generated waves in laboratory channels, J. Waterway, Port, Coastal & Ocean Eng. 106 (1980) 79–96.
[22] L. Shemer, M. Chamesse, Experiment on nonlinear gravity-capillary waves, J. Fluid Mech. 380 (1999) 205–232.
[23] E. Kit, L. Shemer, On dissipation coefficients in a wave tank, Acta Mech. 77 (1989) 171–180.
[24] L. Shemer, E. Kit, T. Miloh, Measurements of two- and three-dimensional waves in a channel including the vicinity of cut-off frequencies, Exp. Fluids 5 (1987) 66–72.